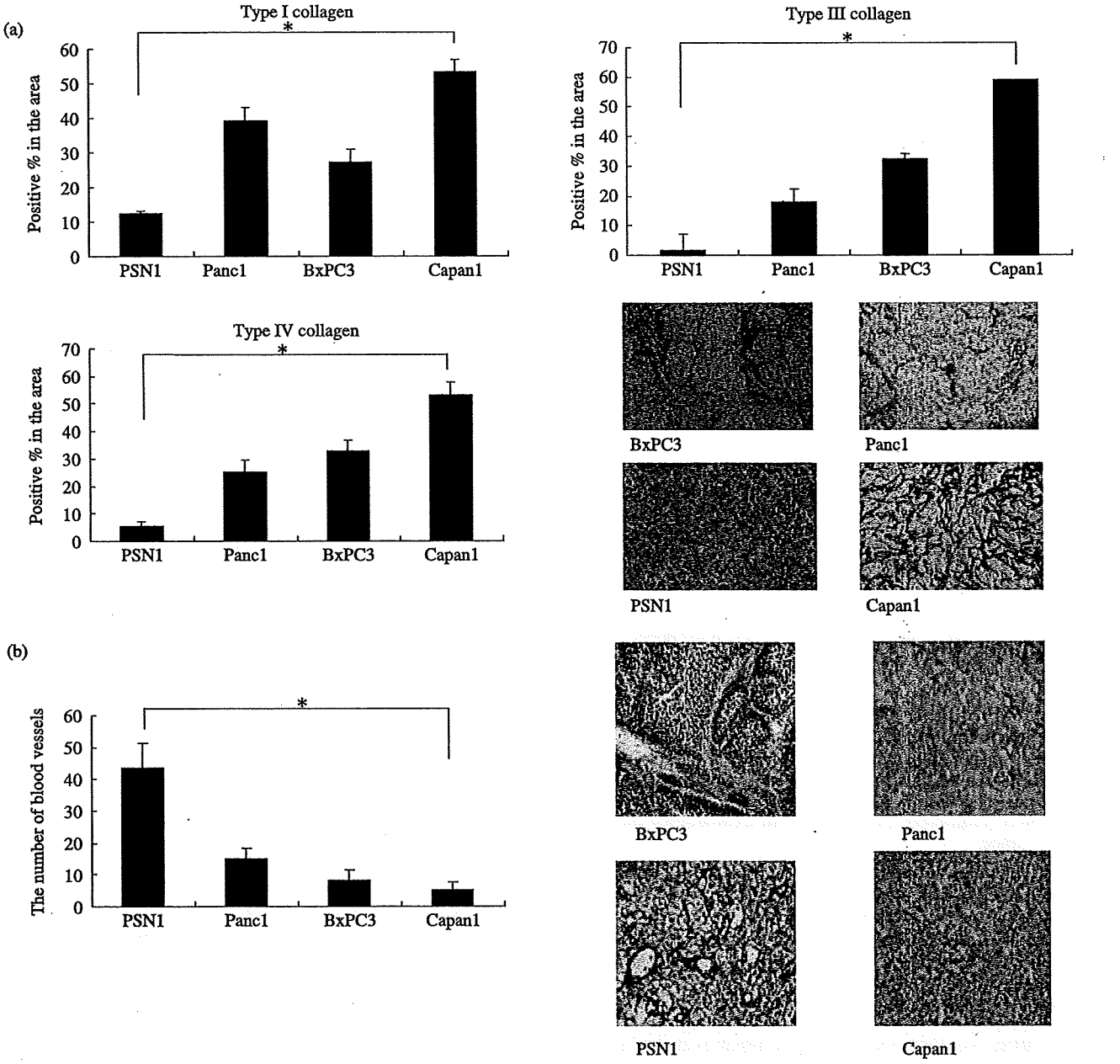

Fig. 1. Examination of the amount of stroma and the number of tumor blood vessels in four human pancreatic cancer xenografts. (a) The amount of stroma in the four xenografts BxPC3, Panc1, PSN1, and Capan1. Immunohistochemical staining was conducted in order to determine the distribution of type I, III, and IV collagen in the tumors. The area occupied by each of type I collagen (left, upper), type III collagen (right, upper), and type IV collagen (left, bottom) was quantified. A representative immunostained image for type IV collagen is shown (right, bottom). (b) The number of blood vessels in the four xenografts. After immunostaining with anti-factor VIII antibody, the number of tumor blood vessels in each of the xenografts was counted. $*P < 0.05$. Bar = SD.

Capan1 exhibited the highest density of type III collagen, and BxPC3 and PSN1 were in second and fourth place, respectively, with respect to the density of type III collagen. The distribution of type IV collagen tended to be similar to that of type I and III collagen.

We also examined the number of tumor blood vessels (Fig. 1b). The PSN1 tumor possessed the largest number of blood vessels among the tumors. In contrast, the Capan1 xenografts had the smallest number of tumor blood vessels.

We have summarized the results on collagen density and blood vessel number obtained in our study for each pancreatic xenograft. Capan1 was the most collagen-rich tumor, and the density of collagen was lowest in PSN1. In contrast, tumor blood vessels were most abundant in PSN1 and least abundant in Capan1. Therefore, we decided to use Capan1 as a hypovascular tumor model and PSN1 as a hypervascular tumor model.

***In vitro* cytotoxic effects of NK012, SN-38, and CPT-11 against the Capan1 and PSN1 cell lines.** The 50% inhibitory concentration (IC_{50}) values of NK012 for the two cell lines, Capan1 (Fig. 2a) and PSN1 (Fig. 2b), ranged from 0.001 to 0.1 μM. NK012 exhibited a remarkably higher cytotoxic effect against both of the cell lines compared with CPT-11. In contrast the cytotoxic effect of SN-38 was similar to that of NK012. The IC_{50} value of each drug against PSN1 was almost similar to that of Capan1.

Antitumor activity analysis of NK012 and CPT-11 using Capan1- and PSN1-bearing nude mice. Antitumor activity was observed in mice treated with NK012 at a dose of 30 mg/kg/d and CPT-11

doi: 10.1111/j.1349-7006.2008.00806.x

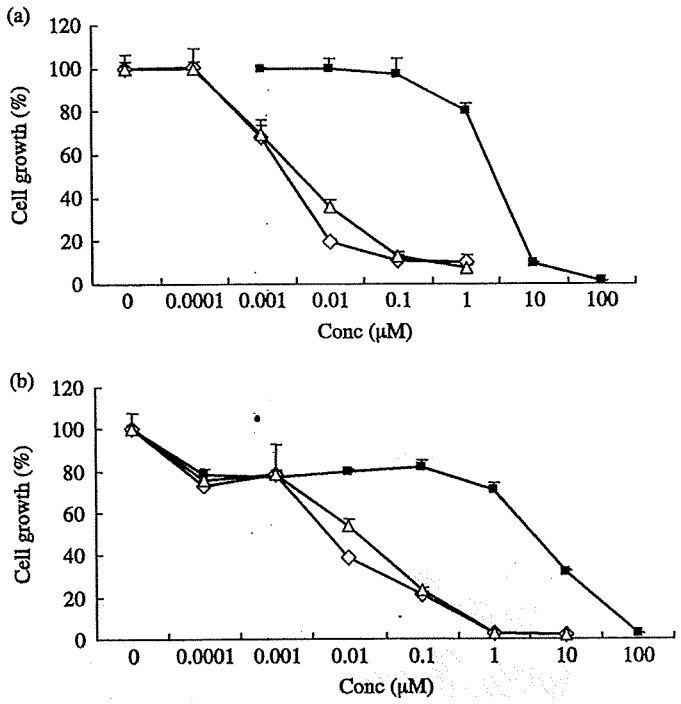

Fig. 2. (a) Capan1 and (b) PSN1 cells were exposed to the indicated concentrations of each drug for 72 h. The growth inhibition curves for NK012 (△), SN-38 (◇), and CPT-11 (■) are shown.

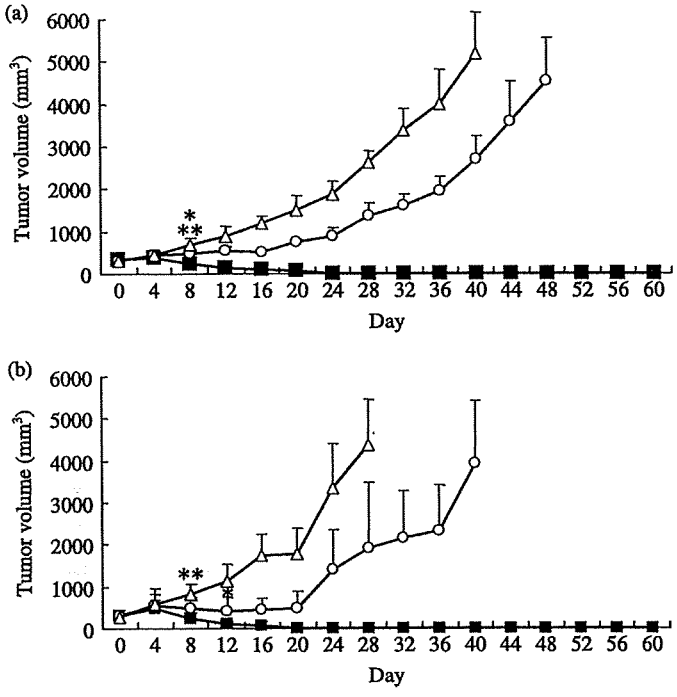

Fig. 3. Antitumor effect of NK012 and CPT-11. NK012 (■), CPT-11 (○), or saline (△) was administered intravenously. When the mean tumor volumes reached 300 mm³ (on day 0), NK012 (30 mg/kg/day) or CPT-11 (66.7 mg/kg/day) was administered on days 0, 4, and 8. Each group consisted of five mice. (a) Capan1 tumor; (b) PSN1 tumor. $*P < 0.05$ (NK012 vs CPT11); $**P < 0.05$ (NK012 vs saline).

at a dose of 66.7 mg/kg/d *in vivo* (Fig. 3). Although CPT-11 exerted a significant antitumor effect compared with the control group in mice bearing the Capan1 tumor, the tumor volume continued to increase consistently. However, in the mice treated with NK012, the tumor volume started to shrink on day 8, and the disappeared completely by day 28 in all treated mice bearing the Capan1 tumor.

In contrast to the observations for the Capan1 tumor, mice bearing the PSN1 tumor treated with CPT-11 showed a slight reduction in tumor volume from day 4 to 12. However, after day 12 the tumor volume began to increase again. On the other hand, the tumor disappeared completely in all mice bearing the PSN1 tumor treated with NK012.

Distribution studies of CPT-11 and NK012 in the solid Capan1 and PSN1 tumors. With the purpose of evaluating drug distribution and accumulation over time, sections of the tumor treated with NK012 or CPT-11 were examined by fluorescence microscopy. Also, we examined the number of tumor blood vessels. In sections of the Capan1 tumor treated with CPT-11, maximum drug accumulation was observed within 1 h of the injection of CPT-11 (Fig. 4a). At 6 h after the injection, the fluorescence originating from CPT-11 had almost entirely disappeared. Subsequently, no accumulation of CPT-11 was observed within the tumor tissues. However, in sections of the Capan1 tumor treated with NK012, fluorescence from NK012 began to appear around tumor blood vessels at 1 h after the intravenous injection and lasted until 48 h. After 6 h, the fluorescent area began to increase and the maximum fluorescence area was observed at 24 h after the injection. Similar results were obtained for the PSN1 tumor (Fig. 4b).

These microscopic observations were confirmed quantitatively by measuring the amount of SN-38 that could be extracted from each of the solid tumors by reverse-phase HPLC. Only slight conversion from CPT-11 to SN-38 was seen from 1 to 24 h in the Capan1 tumor and from 1 to 48 h in the PSN1 tumor, and no SN-38 was detected thereafter. In contrast, SN-38 released from NK012 continued to be detected in both tumors from 1 to 96 h after the injection of NK012 (Fig. 5).

Discussion

Recently, several new formulations categorized as DDS have been approved in the field of oncological treatment, such as Doxil, a polyethylene glycol-liposome incorporating adriamycin,[10,11] and abraxane, a taxol coated with albumin.[12,13] In addition, several clinical trials of drugs based on the DDS concept are now underway.[14–16] Because such formulations possess a longer plasma area under the curve (AUC), liposomal drugs should have sufficient time to exit from tumor blood vessel and accumulate at reasonably high dose levels in the surrounding interstitium.

It has been reported that although polyethylene glycol (PEG) liposomes can be delivered efficiently to a solid tumor, free drug is not transferred sufficiently to cancer cells, particularly those that are distant from the tumor vessels, because the formulations are too large to move through the tumor interstitium.[17] Also, it has been suggested that liposomes are too stable to allow the drug within to be released easily. Therefore, it has been speculated that PEG liposomes may not be so effective against cancers in which the tumor vessel network is irregular and loose because of an abundant collagen-rich matrix. Some examples of such cancers include scirrhous cancer of the stomach and pancreatic cancer. In fact, Doxil is known to be clinically effective against ovarian and breast cancers, both of which are characterized by a high density of tumor microvessels, whereas it is not effective against stomach and pancreatic cancers.[18] Therefore, it is conceivable that some special device is necessary for DDS drugs to exert their antitumor effect sufficiently even against hypovascular tumors such as pancreatic cancer.

In the present study, we characterized the tumor vessel and its interstitium using four kinds of human pancreatic xenografts. The results revealed that the number of tumor blood vessels was inversely related to the amount of collagen within the tumor tissues. Among the four cell lines, Capan1 was the poorest in

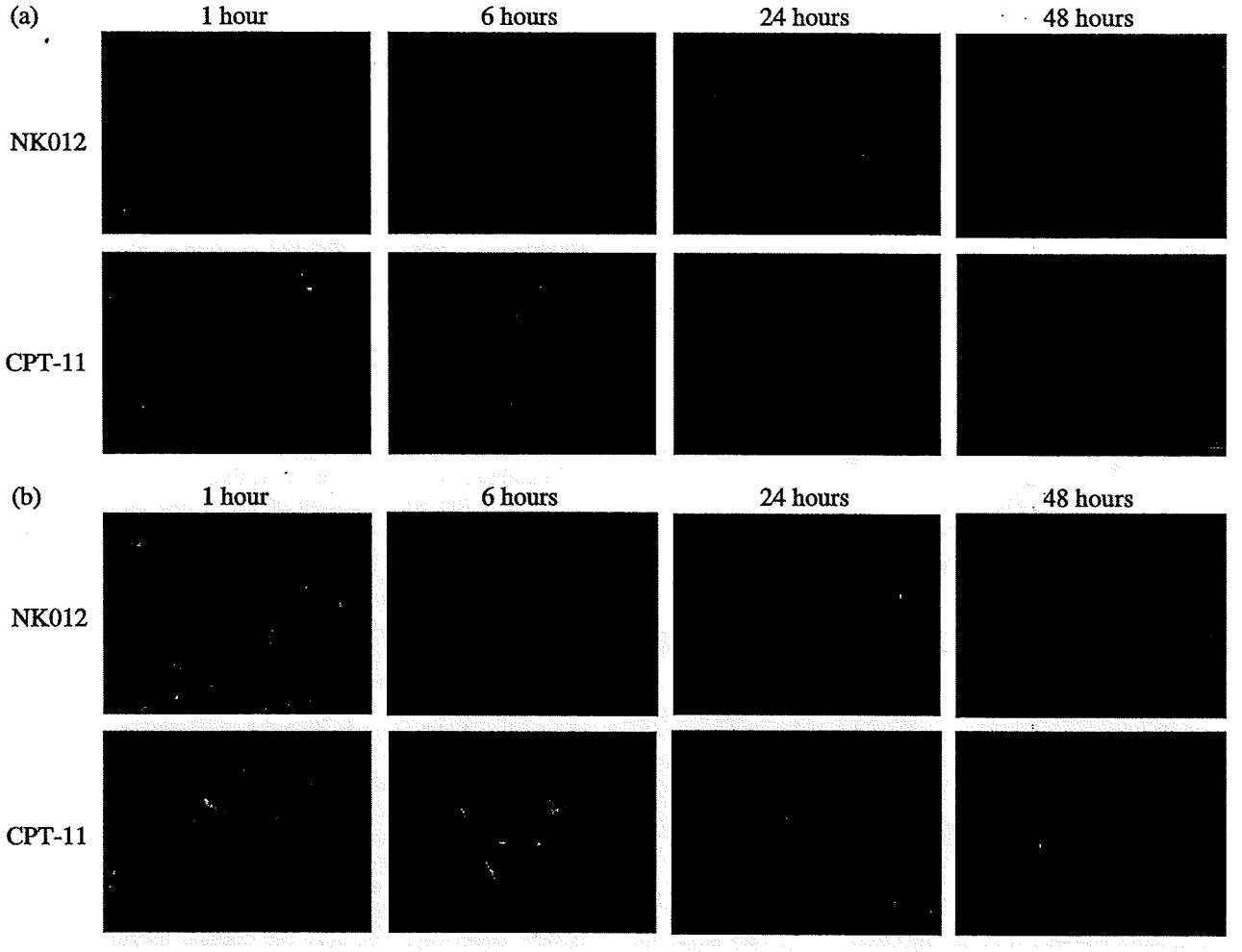

Fig. 4. Distribution of NK012 or CPT-11 in the (a) Capan1 and (b) PSN1 tumor xenografts. Mice bearing Capan1 or PSN1 tumors were injected with NK012 (30 mg/kg/day) or CPT-11 (66.7 mg/kg/day). The tumor tissues were excised at 1, 6, 24, and 48 h after the intravenous injection of NK012 or CPT-11. Each mouse was administered an injection of fluorescein-labeled *Lycopersicon esculentum* lectin just before being killed, for detecting the tumor blood vessels. The frozen sections were examined under a fluorescence microscope at an excitation wavelength of 377 nm and emission wavelength of 447 nm. The same fluorescence conditions can be applied for visualizing NK012 and CPT-11 fluorescence. Free SN-38 can not be detected under these fluorescence conditions.

tumor vasculature and richest in the amount of collagen within the tumor tissue. Conversely, PSN1 was the richest in tumor vasculature and poorest in the amount of collagen. Therefore, it may safely be said that Capan1 xenografts are most like human pancreatic cancer tissue in terms of the amount of interstitial tissue among the four cell lines tested.

We evaluated the *in vitro* cytotoxic effect of CPT-11, SN-38, and NK012 and the *in vivo* antitumor activity of CPT-11 and NK012 against Capan1 tumors as a hypovascular tumor model and PSN1 tumors as a hypervascular tumor model. SN-38 and NK012 exhibited a higher cytotoxic effect against the two cell lines compared with CPT-11. Between SN-38 and NK012, the cytotoxic effect of NK012 was almost similar or a little lower compared with that of SN-38. As CPT-11 itself is a prodrug and is converted to SN-38, an active metabolite of CPT-11, by carboxylesterases, the activity of CPT-11 is dependent on the activity of the enzymes. It is speculated that the efficient sustained release of SN-38 from NK012 allows the formulation to exert a similar cytotoxic effect to that of SN-38. In the *in vivo* experiment, CPT-11 showed significant antitumor activity against both PSN1 tumors as a hypervascular tumor model and Capan1 tumors as a hypovascular tumor model. A slight reduction in tumor size was observed from day 4 to 12 in the case of PSN1 tumors, but not Capan1 tumors. We suggest that the higher antitumor activity seen in PSN1 compared with Capan1 tumors is probably because of the greater accumulation of CPT-11 in the PSN1 xenografts because of the more abundant vasculature. Surprisingly, NK012 could cause complete disappearance of both PSN1 and Capan1 tumor xenografts. Before conducting the experiment, we had anticipated that NK012 might exert stronger antitumor effects against PSN1 compared with Capan1, because such macromolecular drugs can accumulate more efficiently in the PSN1 xenografts because of the richer vasculature. Therefore, we then intensively examined the distribution of NK012 and CPT-11 within the PSN1 or Capan1 xenografts by fluorescence microscopy and HPLC. In the analysis by fluorescence microscopy, NK012 appeared within and around the tumor blood vessels in both the PSN1 and Capan1 xenografts at 1 h after the injection. NK012 began to spread from the blood vessels within the tumor tissue of both xenografts. Fluorescence originating from NK012 increased to a maximum in both of the tumors by 24 h after the injection of NK012. Namely, NK012 was distributed throughout the entire body of both tumors at 24 h after the injection. Furthermore, fluorescence originating from NK012 was clearly and diffusely detected throughout both tumors.

However, fluorescence originating from CPT-11 increased to a maximum at 1 h in both tumors after the injection of CPT-11, indicating that maximum distribution of CPT-11 was achieved

doi: 10.1111/j.1349-7006.2008.00806.x

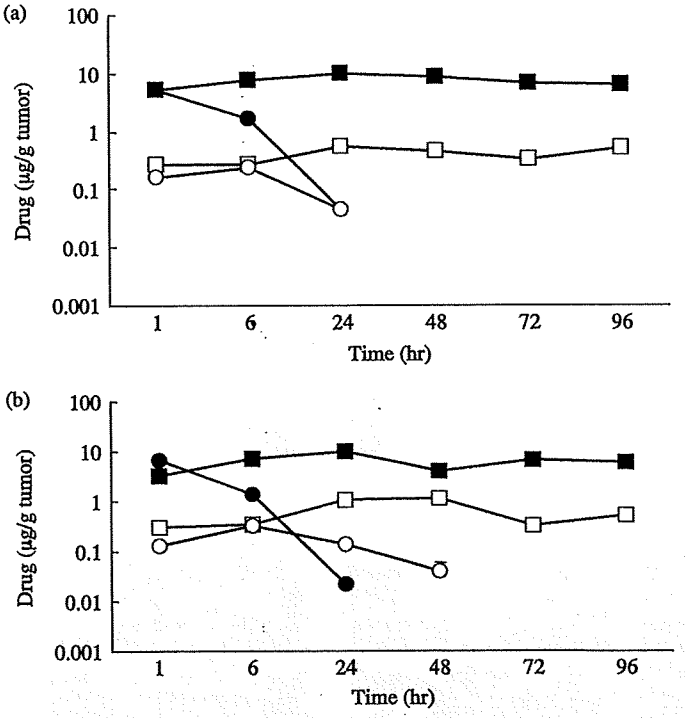

Fig. 5. Tumor distribution of CPT-11, NK012 (or polymer bound SN-38), and free SN-38 after administration of NK012 and CPT-11 to mice bearing (a) Capan1 or (b) PSN1 xenografts. The time profiles of polymer-bound SN-38 (■), free SN-38 released from NK012 (□), CPT-11 (●), and free SN-38 converted from CPT-11 (○) were obtained by high-performance liquid chromatography analysis. The time points examined were 1, 6, 24, 48, 72, and 96 h after the administration of CPT-11 or NK012.

in both tumors within 1 h of the injection. No or very slight fluorescence of CPT-11 was observed in the tumors at 6 h after CPT-11 injection. These observations were confirmed quantitatively by measuring the amount of SN-38 extracted from both tumors by reverse-phase HPLC. Only slight conversion to SN-38 from CPT-11 was seen from 1 to 24 h in the Capan1 tumor and from 1 to 48 h in the PSN1 tumor, and no SN-38 was detected thereafter. SN-38 released from NK012 continued to be detected in both tumors from 1 to 96 h after the injection of NK012. In both CPT-11 and NK012, SN-38 binds to each counter molecule via an ester bond, which confers blue fluorescence on CPT-11 and NK012. Therefore, it is speculated that polymer-bound SN-38 can be distributed throughout the entire body of the tumor, regardless of the amount of interstitial tissue. We are unable to explain clearly how NK012 was distributed well even in hypovascular tumors. However, it is speculated that NK012 can move smoothly within the tumor interstitium because of its relatively small particle size (20 nm) compared with other DDS formulations, and because of its flexibility the formulation can pass through even narrow gaps within the interstitium. Previously, we reported that sustained release of 74% free SN-38 occurred from NK012 under physiological conditions within 48 h.[8] It is also important to remember that the antitumor activity of SN-38 is time dependent.[19] Taking all of these data together, it may be concluded that NK012 can selectively accumulate in pancreatic tumor xenografts, to be distributed effectively throughout the entire body of the tumor, including in hypovascular tumors, and shows sustained release for a prolonged period of time. Consequently, NK012 can exert more significant antitumor activity than CPT-11, which is not an ideal formulation for realizing the time-dependent actions of the drug.

In addition to our present study, there have been several efforts to enhance the accumulation of anticancer agents in tumors to obtain higher antitumor activities of drugs. For example, it has been reported that a transforming growth factor-β inhibitor can enhance tumor vascular permeability to promote accumulation of macromolecules.[20] Conversely, combined use of an antiangiogenic agent, such as an antibody to VEGF, with an anticancer agent could enhance the antitumor activity, probably by lowering the tumor vascular permeability with a consequent decrease in the interstitial fluid pressure so that the anticancer agents may accumulate more easily in the tumor.[21,22] However, much remains to be clarified.

In the present paper, we have shown not only the superiority of the antitumor effect of NK012 compared with that of CPT-11, but also propose that enhanced accumulation, distribution, and retention of DDS within the tumor tissue and the sustained release of anticancer agents from DDS particles are key elements for the treatment of hypovascular tumors. A phase I clinical trial is now underway. Not only the clinical usefulness of NK012, but also the new concept for antitumor actions described in this paper are intended to be verified in the near future through further preclinical and clinical studies.

Acknowledgments

We thank Mrs H. Miyatake and Mrs N. Mie for their technical assistance and Mrs K. Shiina for her secretarial assistance. This work was supported partly by a Grant-in-Aid from the 3rd Term Comprehensive Control Research for Cancer, Ministry of Health, Labor and Welfare (Y. Matsumura) and Scientific Research on Priority Areas from the Ministry of Education, Culture, Sports, Science and Technology (Y. Matsumura).

References

1 Jemal A, Siegel R, Ward E, Murray T, Xu J, Thun MJ. Cancer statistics, 2007. *CA Cancer J Clin* 2007; **57**: 43–66.
2 Burris HA 3rd, Moore MJ, Andersen J *et al.* Improvements in survival and clinical benefit with gemcitabine as first-line therapy for patients with advanced pancreas cancer: a randomized trial. *J Clin Oncol* 1997; **15**: 2403–13.
3 Moore MJ, Goldstein D, Hamm J *et al.* Erlotinib plus gemcitabine compared with gemcitabine alone in patients with advanced pancreatic cancer: a phase III trial of the National Cancer Institute of Canada Clinical Trials Group. *J Clin Oncol* 2007; **25**: 1960–6.
4 Hosoki T. Dynamic CT of pancreatic tumors. *AJR Am J Roentgenol* 1983; **140**: 959–65.
5 Sofuni A, Iijima H, Moriyasu F *et al.* Differential diagnosis of pancreatic tumors using ultrasound contrast imaging. *J Gastroenterol* 2005; **40**: 518–25.
6 Matsumura Y, Maeda H. A new concept for macromolecular therapeutics in cancer chemotherapy: mechanism of tumoritropic accumulation of proteins and the antitumor agent smancs. *Cancer Res* 1986; **46**: 6387–92.
7 Muggia FM. Doxorubicin-polymer conjugates: further demonstration of the concept of enhanced permeability and retention. *Clin Cancer Res* 1999; **5**: 7–8.
8 Koizumi F, Kitagawa M, Negishi T *et al.* Novel SN-38-incorporating polymeric micelles, NK012, eradicate vascular endothelial growth factor-secreting bulky tumors. *Cancer Res* 2006; **66**: 10 048–56.
9 Kawato Y, Furuta T, Aonuma M, Yasuoka M, Yokokura T, Matsumoto K. Antitumor activity of a camptothecin derivative, CPT-11, against human tumor xenografts in nude mice. *Cancer Chemother Pharmacol* 1991; **28**: 192–8.
10 Muggia FM. Liposomal encapsulated anthracyclines: new therapeutic horizons. *Curr Oncol Rep* 2001; **3**: 156–62.
11 Ferrari M. Cancer nanotechnology: opportunities and challenges. *Nat Rev Cancer* 2005; **5**: 161–71.
12 Green MR, Manikhas GM, Orlov S *et al.* Abraxane, a novel Cremophor-free, albumin-bound particle form of paclitaxel for the treatment of advanced non-small-cell lung cancer. *Ann Oncol* 2006; **17**: 1263–8.
13 Gradishar WJ, Tjulandin S, Davidson N *et al.* Phase III trial of nanoparticle albumin-bound paclitaxel compared with polyethylated castor oil-based paclitaxel in women with breast cancer. *J Clin Oncol* 2005; **23**: 7794–803.
14 Matsumura Y, Hamaguchi T, Ura T *et al.* Phase I clinical trial and pharmacokinetic evaluation of NK911, a micelle-encapsulated doxorubicin. *Br J Cancer* 2004; **91**: 1775–81.

15 Hamaguchi T, Matsumura Y, Suzuki M *et al.* NK105, a paclitaxel-incorporating micellar nanoparticle formulation, can extend *in vivo* antitumour activity and reduce the neurotoxicity of paclitaxel. *Br J Cancer* 2005; **92**: 1240–6.
16 Uchino H, Matsumura Y, Negishi T *et al.* Cisplatin-incorporating polymeric micelles (NC-6004) can reduce nephrotoxicity and neurotoxicity of cisplatin in rats. *Br J Cancer* 2005; **93**: 678–87.
17 Unezaki S, Maruyama K, Hosoda J *et al.* Direct measurement of the extravasation of polyethylene glycol-coated liposomes into solid tumour tissue by *in vivo* fluorescence microscopy. *Int J Pharmacol* 1996; **144**: 11–17.
18 Tsukioka Y, Matsumura Y, Hamaguchi T, Koike H, Moriyasu F, Kakizoe T. Pharmaceutical and biomedical differences between micellar doxorubicin (NK911) and liposomal doxorubicin (Doxil). *Jpn J Cancer Res* 2002; **93**: 1145–53.
19 Kawato Y, Aonuma M, Hirota Y, Kuga H, Sato K. Intracellular roles of SN-38, a metabolite of the camptothecin derivative CPT-11, in the antitumor effect of CPT-11. *Cancer Res* 1991; **51**: 4187–91.
20 Kano MR, Bae Y, Iwata C *et al.* Improvement of cancer-targeting therapy, using nanocarriers for intractable solid tumors by inhibition of TGF-β signaling. *Proc Natl Acad Sci USA* 2007; **104**: 3460–5.
21 Jain RK. Normalizing tumor vasculature with anti-angiogenic therapy: a new paradigm for combination therapy. *Nat Med* 2001; **7**: 987–9.
22 Jain RK. Normalization of tumor vasculature: an emerging concept in antiangiogenic therapy. *Science* 2005; **307**: 58–62.

doi: 10.1111/j.1349-7006.2008.00806.x

Novel SN-38–Incorporated Polymeric Micelle, NK012, Strongly Suppresses Renal Cancer Progression

Makoto Sumitomo,[1] Fumiaki Koizumi,[2] Takako Asano,[1] Akio Horiguchi,[1] Keiichi Ito,[1] Tomohiko Asano,[1] Tadao Kakizoe,[3] Masamichi Hayakawa,[1] and Yasuhiro Matsumura[4]

[1]Department of Urology, National Defense Medical College, Tokorozawa, Saitama, Japan; [2]Shien-Lab, Medical Oncology, National Cancer Center Hospital; [3]National Cancer Center, Tokyo, Japan; and [4]Investigative Treatment Division, Research Center for Innovative Oncology, National Cancer Center Hospital East, Chiba, Japan

Abstract

It has been recently reported that NK012, a 7-ethyl-10-hydroxy-camptothecin (SN-38)–releasing nanodevice, markedly enhances the antitumor activity of SN-38, especially in hypervascular tumors through the enhanced permeability and retention effect. Renal cell carcinoma (RCC) is a typical hypervascular tumor with an irregular vascular architecture. We therefore investigated the antitumor activity of NK012 in a hypervascular tumor model from RCC. Immunohistochemical examination revealed that Renca tumors contained much more CD34-positive neovessels than SKRC-49 tumors. Compared with CPT-11, NK012 had significant antitumor activity against both bulky Renca and SKRC-49 tumors. Notably, NK012 eradicated rapid-growing Renca tumors in 6 of 10 mice, whereas it failed to eradicate SKRC-49 tumors. In the pulmonary metastasis treatment model, an enhanced and prolonged distribution of free SN-38 was observed in metastatic lung tissues but not in nonmetastatic lung tissues after NK012 administration. NK012 treatment resulted in a significant decrease in metastatic nodule number and was of benefit to survival. Our study shows the outstanding advantage of polymeric micelle-based drug carriers and suggests that NK012 would be effective in treating disseminated RCCs with irregular vascular architectures. [Cancer Res 2008;68(6):1631–5]

Introduction

Passive targeting of the drug delivery system is suited to combating the pathophysiologic characteristics present in many solid tumors: hypervascularity, irregular vascular architecture, potential for secretion of vascular permeability factors, and the absence of effective lymphatic drainage that prevents efficient clearance of macromolecules. These characteristics, unique to solid tumors, are believed to be the basis of the enhanced permeability and retention (EPR) effect (1). Polymeric micelle-based anticancer drugs have recently been developed (2, 3), and some were put under evaluation for clinical trials (4, 5).

7-Ethyl-10-hydroxy-camptothecin (SN-38), a biological active metabolite of irinotecan hydrochloride (CPT-11), has potent antitumor activity, but has not been used clinically because it is a water-insoluble drug. It has been recently shown that novel SN38-incorporated polymeric micelles, NK012, have the potential to allow effective sustained release of SN-38 inside a tumor and possess potent antitumor activities especially in a vascular endothelial growth factor (VEGF)–secreting hypervascular tumor (6), because the supramolecular structures of NK012 which enable SN-38 to accumulate in the target tissue are based on the EPR effect (1).

Renal cell carcinoma (RCC) is a typical hypervascular tumor with an irregular vascular architecture. We therefore conducted an investigation to determine whether NK012 would be effective in treating RCC by using established RCC tumor models with pulmonary metastasis.

Materials and Methods

Drugs and cells. CPT-11 was purchased from Yakult Honsha Co., Ltd. SN-38 and NK012 was prepared and supplied by Nippon Kayaku Co., Ltd. (6). Five human RCC lines (SKRC-49, Caki-1, 769P, 786O, and KU19-20) and murine Renca cells were maintained in DMEM or MEM supplemented with 2 mmol/L glutamine, 1% nonessential amino acids, 100 units/mL streptomycin and penicillin, and 10% FCS.

***In vitro* growth inhibition assay.** The growth inhibitory effects of NK012, SN-38, and CPT-11 were examined with a 3-(4, 5-dimethylthiazol-2-yl)-2, 5-diphenyltetrazolium bromide (MTT) assay, as described previously (6).

***In vivo* growth inhibition assay.** The animal experimental protocols were approved by the Committee for Ethics of Animal Experimentation, and the experiments were conducted in accordance with the Guidelines for Animal Experiments in the National Cancer Center. Athymic nude mice (3–4 wk old) were maintained in a laminar air flow cabinet under aseptic conditions. 10^7 RCC cells were s.c. injected into the backs of the mice. NK012 at doses of 10 mg/kg/d or 20 mg/kg/d and CPT-11 at doses of 15 mg/kg/d or 30 mg/kg/d were given i.v. on days 0 (when tumors were allowed to grow until they became massive in size, around 1.5 cm), 4, and 8. Tumor volume was determined by direct measurement with calipers and calculated as $\pi/6 \times (\text{large diameter}) \times (\text{small diameter})^2$.

Assessment of treatment effects of NK012 on murine pulmonary metastasis model. A total of 1×10^5 Renca cells were inoculated into male BALB/c mice via the tail vein. The mice were randomly divided into three groups of 10. NK012 at dose of 20 mg/kg/d and CPT-11 at dose of 30 mg/kg/d were given i.v. on days 0 (7 d after inoculation), 4, and 8. After that, the mice were sacrificed, their lungs were stained intratracheally with 15% India black ink solution, and the number of metastatic nodules in each mouse was counted. To determine the effect of NK012 on survival, an identical experiment to the one described above was done. After treatment, mice were maintained until each animal showed signs of morbidity (i.e., over 10% weight loss compared with untreated controls), at which point they were sacrificed. Kaplan-Meier analysis was done to determine the effect on time to morbidity, and statistical differences were ranked according to a Mantel-Cox log-rank test using the StatView 5.0 software package.

Histologic and immunohistochemical analysis. Histologic sections were taken from Renca tumor tissues. After extirpation, tissues were fixed with 3.9% formalin in PBS (pH 7.4), and the subsequent preparations and H&E staining were performed by Tokyo Histopathological Laboratory Co.,

Requests for reprints: Yasuhiro Matsumura, Investigative Treatment Division, Research Center for Innovative Oncology, National Cancer Center Hospital East, 6-5-1 Kashiwanoha, Kashiwa City, Chiba 277-8577, Japan. Phone: 81-4-7134-6857; Fax: 81-4-7134-6857; E-mail: yhmatsum@east.ncc.go.jp.

doi:10.1158/0008-5472.CAN-07-6532

Table 1. *In vitro* growth inhibitory activity of SN-38, NK012, and CPT-11 in RCC lines (MTT assay)

Cell line	IC_{50} (μmol/L)		
	SN-38	NK012*	CPT-11
SKRC-49	0.0064 ± 0.005	0.011 ± 0.008	4.14 ± 0.45
Caki-1	0.0062 ± 0.009	0.032 ± 0.006	8.45 ± 0.85
769P	0.015 ± 0.007	0.085 ± 0.014	34.54 ± 3.76
786O	0.031 ± 0.007	0.12 ± 0.012	28.14 ± 1.21
KU19-20	0.10 ± 0.006	0.34 ± 0.014	32.65 ± 1.25
Renca	0045 ± 0.005	0.0096 ± 0.008	2.26 ± 0.05

*The dose of NK012 is expressed as a dose equivalent to SN-38.

Ltd. Monoclonal anti-CD34 antibody (HyCult Biotechnology) was used to detect the tumor blood vessels. CD34-positive neovessels were counted in 10 high-power fields (×400) by two independent investigators who operated in a blinded fashion.

Assay for free (polymer-unbound) SN-38 in lung tissues. The Renca pulmonary metastasis model described above was used for the analysis of the biodistribution of NK012 and CPT-11. Ten days after Renca inoculation, NK012 (20 mg/kg) or CPT-11 (30 mg/kg) was given i.v. to the mice. The mice were sacrificed at 0, 24, 48, and 72 h after administration, and lung samples were taken and stored at −80°C until analysis. We prepared control mice without Renca inoculation as the nonmetastatic model; NK012 was administrated as well, and lung samples were stored. Samples were then homogenized on ice using a Digital homogenizer (Iuchi) and suspended in the mixture of 100 mmol/L glycine-HCl buffer (pH 3)/methanol (1:1, v/v) at a concentration of 5% w/w. Proteins were precipitated with an ice-cold mixture of 1 mmol/L H_3PO_4/MeOH/H_2O (1:1:4, v/v/v) containing camptothecin as an I.S. The sample was vortexed for 10 s and filtered through a MultiScreen Solvinert (Millipore Corporation), and the concentration of free SN-38 in the aliquots of the homogenates (100 μL) was determined using the high-performance liquid chromatography method (6).

Statistical analysis. Data were expressed as mean ± SD. Significance of differences was calculated using the unpaired *t* test with repeated measures of StatView 5.0. $P < 0.05$ was regarded as statistically significant.

Results and Discussion

We first evaluated *in vitro* cellular sensitivity of RCC lines to SN-38, NK012, and CPT-11. The IC_{50} values of each agent for RCC lines are shown in Table 1. NK012 exhibited higher cytotoxic effect against each cell line compared with CPT-11 (96-fold to 406-fold sensitive).

It is essential to elucidate the correlation between the effectiveness of micellar drugs and tumor hypervascularity and hyperpermeability. Gross evaluation of those RCC tumors s.c. injected into the backs of mice revealed that Renca tumors were more reddish and grew faster than SKRC-49 tumors, and immunohistochemical examination showed that Renca tumors contained much more CD34-positive neovessels than SKRC-49 tumors (Fig. 1).

We allowed the tumors to grow until they became massive, around 1.5 cm, and then initiated treatment. A striking decrease in Renca tumor volume was observed on day 15 in mice treated with NK012 at 20 mg/kg/d compared with the untreated control (Fig. 2*A*). Renca bulky masses completely disappeared on day 21 in 6 of 10 mice treated with NK012 at 20 mg/kg/d. On the other hand, Renca tumors in mice treated with CPT-11 at 30 mg/kg/d were not eradicated and rapidly regrew after a partial response at day 15. An approximate 10% body weight loss occurred in mice treated with NK012 20 mg/kg, compared with the untreated controls, but there was no significant difference in comparison with tumor-free mice treated with NK012, suggesting that the decrease in body weight was likely to be due to tumor shrinkage rather than toxic effects. We next compared the antitumor activities of the NK012 and CPT-11 treatment in SKRC-49 and Renca tumors. The SKRC-49 tumor volume in mice treated with NK012 at 20 mg/kg/d on day 21 was over 70% smaller than in the untreated controls on day 21 and ~50% smaller than in mice on day 0 (Fig. 2*B*). However, the SKRC-49 tumors were not eradicated in mice treated with NK012. Considering that equivalent *in vitro* growth inhibitory effects by NK012 were observed for SKRC-49 and Renca cells (Table 1), our results suggest that the antitumor activity of NK012 *in vivo* might be affected by tumor environment factors, such as tumor vascularity.

We next examined the distribution of free SN-38 in the metastatic or nonmetastatic (no inoculation of Renca cells) lung tissues after administration of NK012 or CPT-11. In the case of NK012 administration in mice with lung metastasis, free SN-38 was detectable at the concentration of >100 ng/g in metastatic lung tissues with a typical microvascular architecture (Fig. 3*A*) even at 72 hours after administration, whereas the concentrations of free SN-38 in nonmetastatic lung tissues after NK012 administration were much lower than those in metastatic lung tissues after treatment with NK012 (significant at 24, 48, and 72 hours; $P < 0.05$;

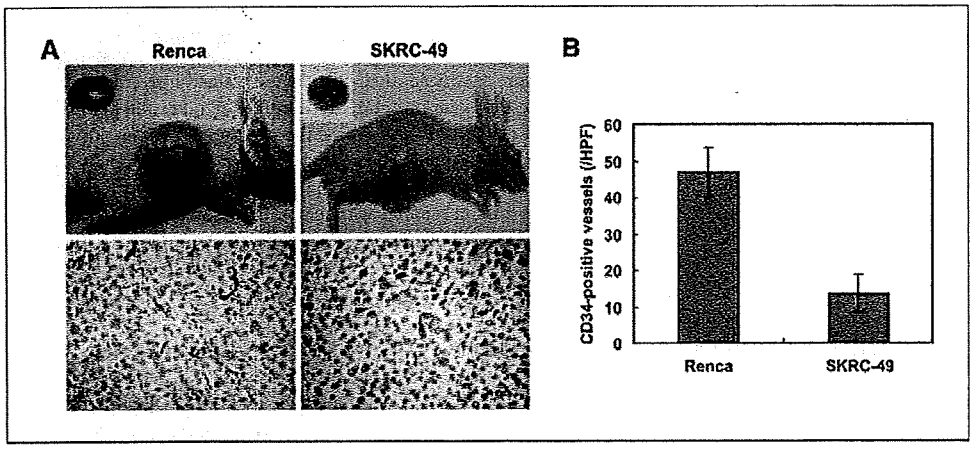

Figure 1. Comparison of tumor angiogeneses of Renca and SKRC-49 in athymic nude mice. *A*, representative photographs of massive tumors developed from Renca and SKRC-49 at 28 d after s.c. injection (inoculation). Immunohistochemical (CD34, ×400) examinations for each tumor are shown. *B*, tumor neovascularization in each tumor was quantified by counting CD34-positive neovessels. *Bars*, SD. Experiments were repeated twice with similar results.

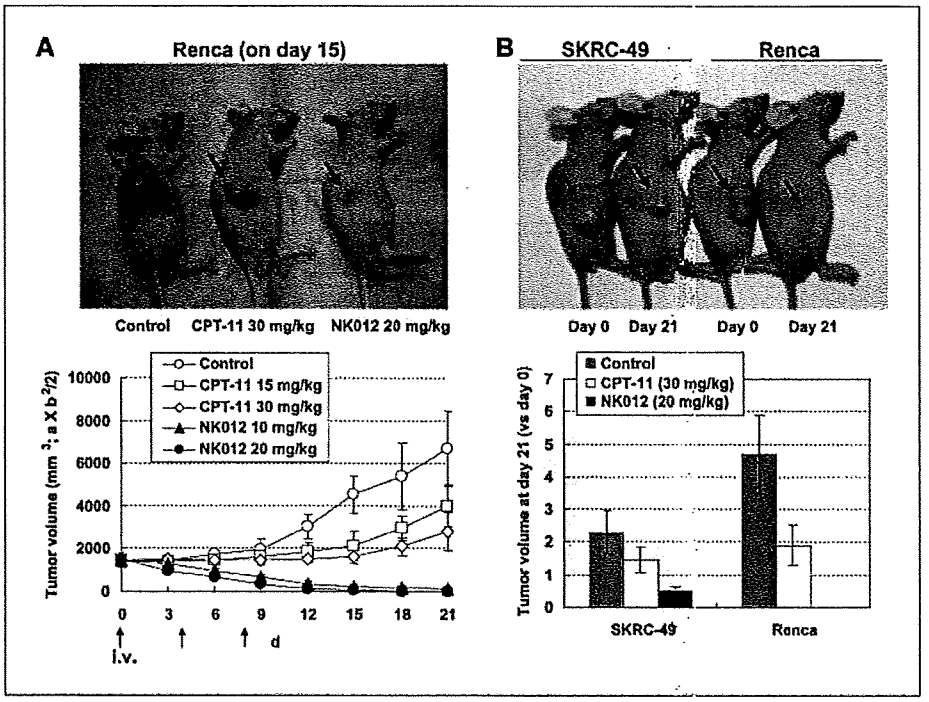

Figure 2. Growth-inhibitory effect of NK012 and CPT-11 on bulky RCC tumors. I.v. administration of NK012 or CPT-11 was started when the mean tumor volumes of groups reached a massive 1,500 mm^3. The mice were divided into test groups as indicated. *A*, representative of each group at day 15 in the Renca allograft model. *Arrows*, Renca allografts (*top*). Time profile of tumor volume in mice treated with NK012 or CPT-11 at indicated doses (*bottom*). Each group consisted of 10 mice. *Bars*, SD. *B*, the comparison of antitumor activities of CPT-11 and NK012 in SKRC-49 xenografts and Renca allografts. Representative of mice treated with NK012 at day 0 and day 21. Experiments were repeated twice with similar results. The mice at day 0 in the photograph belong to the group in the second experiment which started just at day 21 of the first experiment. *Arrows*, tumor grafts. The relative tumor volume values at day 21 to those at day 0 in each group set to 1 (*bottom*). Each group consisted of 10 mice.

Fig. 3*B*). On the other hand, the concentrations of free SN-38 after administration of CPT-11 were almost negligible in metastatic lung tissues at all time points (data not shown). These results strongly suggest that SN-38 could be selectively released from NK012 and maintained in metastatic Renca tumor tissues.

Deviating from the ordinary experimental pulmonary metastasis prevention model, we initiated treatment 7 days after inoculation (day 0) when multiple lung nodules derived from Renca were observed in all mice in our preliminary study (Fig. 4*A*). On day 21, there was no significant difference between the mean number of metastatic nodules in the control group (287 ± 56 nodules, $n = 10$) and in the group receiving CPT-11 treatment (236 ± 59 nodules, $n = 10$). Significant treatment effects were found, however, in the group receiving NK012 treatment (32 ± 18 nodules, $n = 10$) on day 21 compared with the control group on day 21 ($P < 0.0001$). Notably, a dramatic decrease in metastatic nodule number was observed in the NK012 treatment group on day 21 compared with the control group on day 0 (126 ± 23 nodules, $n = 10$, $P < 0.001$; Fig. 4*A*). Kaplan-Meier analysis showed that a significant survival benefit was obtained in the NK012 treatment group compared with

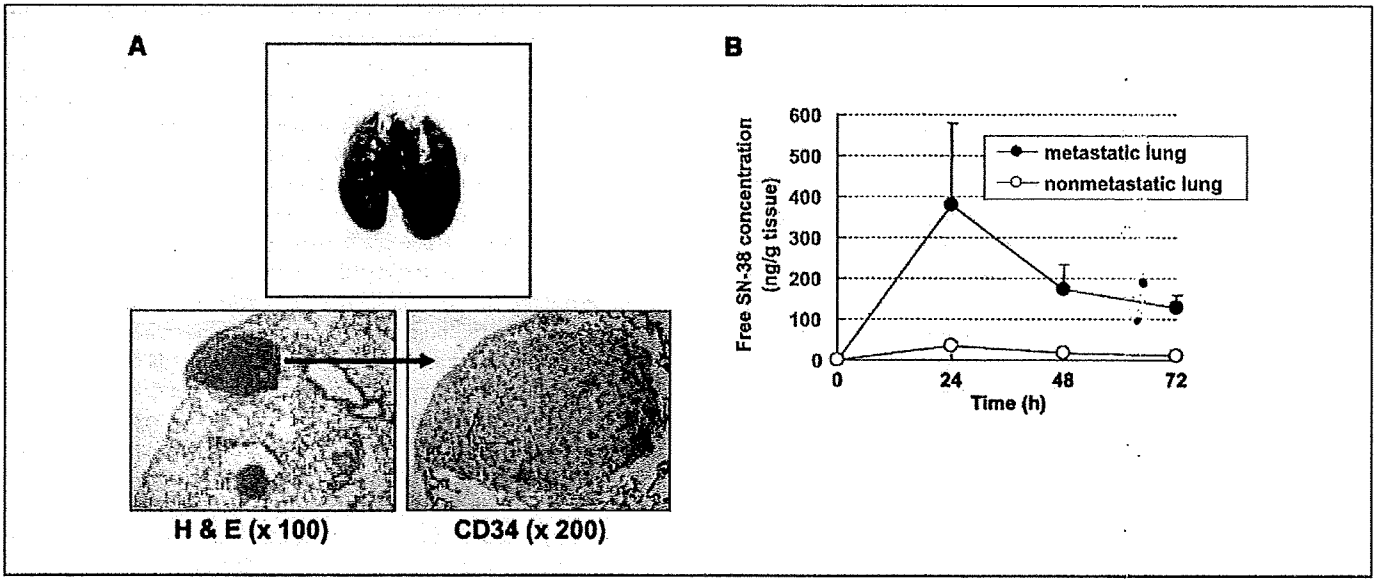

Figure 3. Pulmonary metastasis of Renca cells and lung tissue distribution of free SN-38 after administration of NK012 and CPT-11. *A*, gross appearances of pulmonary metastasis observed 7 d after Renca inoculation (*top*). Multiple metastatic nodules and neovascularization in metastatic lung tumor lesion (*bottom*). *B*, time profile of free SN-38 concentration in metastatic or nonmetastatic lung tissues in mice treated with NK012 (20 mg/kg/d). *Bars*, SD. Experiments were performed in tetraplicate.

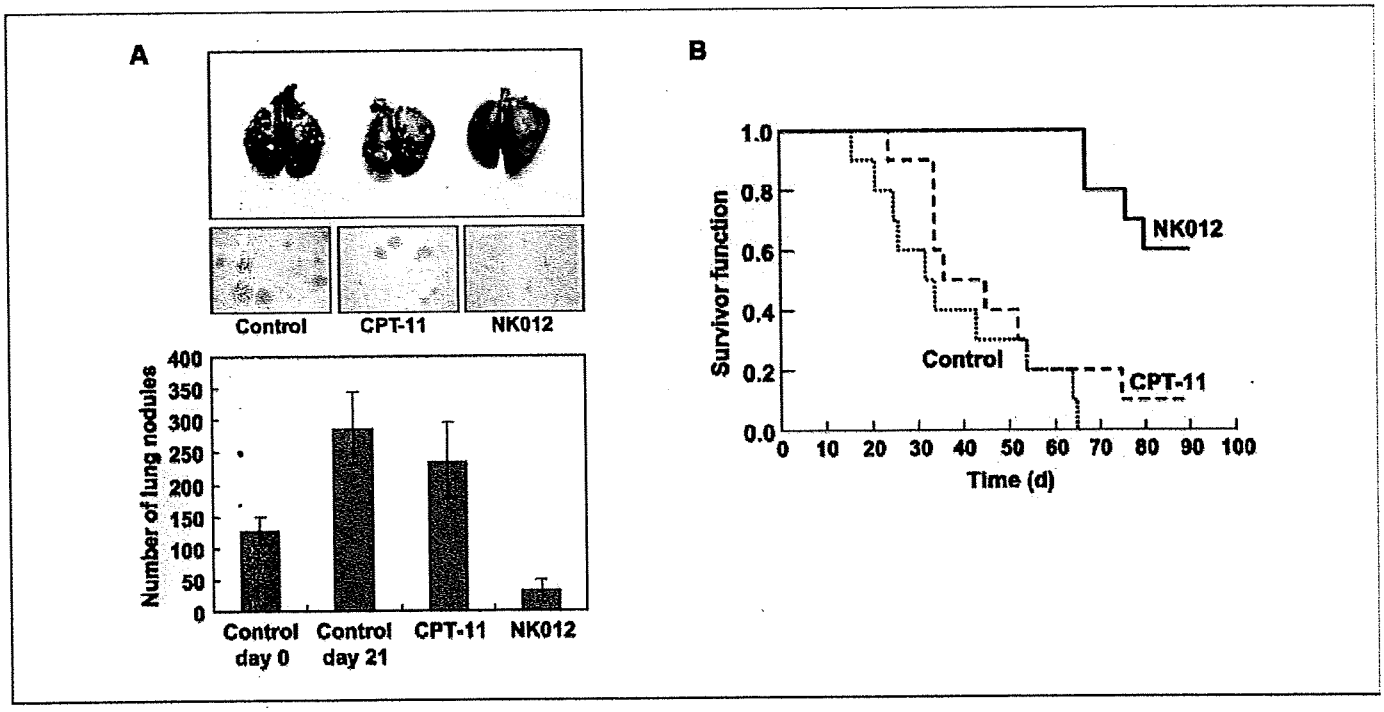

Figure 4. Treatment effect of NK012 on established pulmonary metastasis and survival. NK012 (20 mg/kg/d) and CPT-11 (30 mg/kg/d) were given i.v. to mice with established pulmonary metastasis on days 0 (7 d after Renca inoculation), 4, and 8. *A*, gross and histologic appearances of pulmonary metastases at day 21 (*top*). The metastatic nodules in each mouse were counted. Each group consisted of five mice. *B*, mice were maintained for 90 d after each treatment and survival was assessed by a Kaplan-Meier analysis. Each group consisted of five mice. Experiments were repeated twice with similar results.

the control group ($P < 0.001$), but no significant survival benefit was obtained in CPT-11 treatment group ($P = 0.239$; Fig. 4*B*). Although no severe toxic effects were observed in any mouse treated with NK012, 3 of 10 mice treated with NK012 were sacrificed during the observation period according to the 'Guidelines for Animal Experiments because their body weights had become 10% lower than those of the other mice. However, the sacrificed mice were a little bit smaller than others when they started treatment, and they showed no disseminated lung metastasis (data not shown).

Our results presented here strongly support recent findings reported by us that the macromolecular drug distribution throughout the tumor site was enhanced by the hypervascularity and hyperpermeability, and subsequently higher antitumor activity was achieved (6). We assume that conventional low molecular size anticancer agents almost disappear from the bloodstream without being subjected to the EPR effect before they can reach the target organs (solid tumor). The clinical importance of angiogenesis in human tumors has been shown in several reports indicating a positive relationship between the blood vessel density in the tumor mass and poor prognosis with chemoresistance in patients with various cancers (7–9). Furthermore, recent reports showing that anticancer agents were less active against VEGF-overexpressing tumors (10, 11) may support the idea that low-molecular drugs are not so effective in the treatment of solid tumors which are rich in blood vessels.

Our study thus far has several limitations about clarifying whether extensive angiogenesis in the tumor is an essential determinant for the susceptibility to NK012. In our ongoing study, we found that NK012 also has a striking antitumor activity against some hypovascular tumor models of human pancreatic cancer xenografts.[5] It also remains unclear whether NK012 possesses strong antitumor activity in other metastatic sites besides the lung. It is known that the EPR effect is affected by various permeability factors, such as bradykinin (12), nitric oxide (13). and various cytokines independent of VEGF and hypervascularity (14). Among solid tumors with rapid progression potential, irregularity occurs not only in blood flow and vascular density, but also in the vascular network and anatomic architecture (15, 16), suggesting that EPR effect may be predominantly promoted in rapid-progressive tumor phenotypes and influenced by organ-specific tumor microenvironment. Hoffman and coworkers (17, 18) have developed a technique of surgical orthotopic implantation (SOI) with more clinical features of systemic and aggressive metastases than our conventional animal models. Further preclinical studies using such models as SOI might clarify cancer phenotypes and metastatic organs to which we can apply NK012 more precisely.

The results of chemotherapy in RCCs have been disappointing, as indicated by the low response proportions. However, clinical trials using gemcitabine-containing regimens have been encouraging, with major responses occurring in 5% to 17% of patients (19, 20), suggesting the possibility that chemotherapy is promising as a modality for RCC therapy if anticancer agents can be selectively delivered, released, and maintained around tumor tissues. Our current report highlights the advantages of polymeric micelle-based drug carriers like NK012 as promising modalities for treatment, rather than prevention, of disseminated RCCs with abnormal vascular architecture. The results of our ongoing phase-I

[5] Y. Saito, M. Yasumaga, J. Kuroda, Y. Koga, and Y. Matsumura. Unpublished data.

clinical trial and future phase-II trials of NK012 in patients with advanced solid tumors including RCC might meet or even exceed our expectations.

Acknowledgments

Received 12/10/2007; revised 1/25/2008; accepted 1/31/2008.

Grant support: Grant-in-aid from 3rd Term Comprehensive Control Research for Cancer, Ministry of Health, Labor and Welfare (Y. Matsumura) and Scientific Research on Priority Areas from the Ministry of Education, Culture, Sports, Science and Technology (Y. Matsumura).

The costs of publication of this article were defrayed in part by the payment of page charges. This article must therefore be hereby marked *advertisement* in accordance with 18 U.S.C. Section 1734 solely to indicate this fact.

We thank H. Miyatake and N. Mie for their technical assistance and K. Shiina for her secretarial assistance.

References

1. Matsumura Y, Maeda H. A new concept for macromolecular therapeutics in cancer chemotherapy: mechanism of tumoritropic accumulation of proteins and the antitumor agent smancs. Cancer Res 1986;46:6387–92.
2. Yokoyama M, Miyauchi M, Yamada N, et al. Characterization and anticancer activity of the micelle-forming polymeric anticancer drug adriamycin-conjugated poly(ethylene glycol)-poly(aspartic acid) block copolymer. Cancer Res 1990;50:1693–700.
3. Kataoka K, Harada A, Nagasaki Y. Block copolymer micelles for drug delivery: design, characterization and biological significance. Adv Drug Deliv Rev 2001;47:113–31.
4. Matsumura Y, Hamaguchi T, Ura T, et al. Phase I clinical trial and pharmacokinetic evaluation of NK911, a micelle-encapsulated doxorubicin. Br J Cancer 2004;91:1775–81.
5. Hamaguchi T, Kato K, Yasui H, et al. A phase I and pharmacokinetic study of NK105, a paclitaxel-incorporating micellar nanoparticle formulation. Br J Cancer 2007;97:170–6.
6. Koizumi F, Kitagawa M, Negishi T, et al. Novel SN-38-incorporating polymeric micelles, NK012, eradicate vascular endothelial growth factor-secreting bulky tumors. Cancer Res 2006;66:10048–56.
7. Gasparini G, Harris AL. Clinical importance of the determination of tumor angiogenesis in breast carcinoma: much more than a new prognostic tool. J Clin Oncol 1995;13:765–82.
8. Takahashi Y, Kitadai Y, Bucana CD, Cleary KR, Ellis LM. Expression of vascular endothelial growth factor and its receptor, KDR, correlates with vascularity, metastasis, and proliferation of human colon cancer. Cancer Res 1995;55:3964–8.
9. Williams JK, Carlson GW, Cohen C, Derose PB, Hunter S, Jurkiewicz MJ. Tumor angiogenesis as a prognostic factor in oral cavity tumors. Am J Surg 1994;168:373–80.
10. Natsume T, Watanabe J, Koh Y, et al. Antitumor activity of TZT-1027 (Soblidotin) against vascular endothelial growth factor-secreting human lung cancer *in vivo*. Cancer Sci 2003;94:826–33.
11. Zhang L, Hannay JA, Liu J, et al. Vascular endothelial growth factor overexpression by soft tissue sarcoma cells: implications for tumor growth, metastasis, and chemoresistance. Cancer Res 2006;66:8770–8.
12. Matsumura Y, Maruo K, Kimura M, Yamamoto T, Konno T, Maeda H. Kinin-generating cascade in advanced cancer patients and *in vitro* study. Jpn J Cancer Res 1991;82:732–41.
13. Wu J, Akaike T, Hayashida K, et al. Identification of bradykinin receptors in clinical cancer specimens and murine tumor tissues. Int J Cancer 2002;98:29–35.
14. Maeda H, Fang J, Inutsuka T, Kitamoto Y. Vascular permeability enhancement in solid tumor: various factors, mechanisms involved and its implications. Int Immunopharmacol 2003;3:319–28.
15. Suzuki M, Takahashi T, Sato T. Medial regression and its functional significance in tumor-supplying host arteries. A morphometric study of hepatic arteries in human livers with hepatocellular carcinoma. Cancer 1987;59:444–50.
16. Skinner SA, Tutton PJ, O'Brien PE. Microvascular architecture of experimental colon tumors in the rat. Cancer Res 1990;50:2411–7.
17. An Z, Jiang P, Wang X, Moossa AR, Hoffman RM. Development of a high metastatic orthotopic model of human renal cell carcinoma in nude mice: benefits of fragment implantation compared to cell-suspension injection. Clin Exp Metastasis 1999;17:265–70.
18. Hoffman RM. Orthotopic metastatic mouse models for anticancer drug discovery and evaluation: a bridge to the clinic. Invest New Drugs 1999;17:343–59.
19. Rini BI, Vogelzang NJ, Dumas MC, Wade JL III, Taber DA, Stadler WM. Phase II trial of weekly intravenous gemcitabine with continuous infusion fluorouracil in patients with metastatic renal cell cancer. J Clin Oncol 2000;18:2419–26.
20. Nanus DM, Garino A, Milowsky MI, Larkin M, Dutcher JP. Active chemotherapy for sarcomatoid and rapidly progressing renal cell carcinoma. Cancer 2004;101:1545–51.

Low-intensity ultrasound and microbubbles enhance the antitumor effect of cisplatin

Yukiko Watanabe,[1] Atsuko Aoi,[2] Sachiko Horie,[1] Noriko Tomita,[1] Shiro Mori,[3] Hidehiro Morikawa,[3] Yasuhiro Matsumura,[4] Georges Vassaux[5,6] and Tetsuya Kodama[1,7]

[1]Graduate School of Biomedical Engineering, [2]Graduate School of Dentistry, Tohoku University, [3]Tohoku University Hospital, Sendai, Miyagi 980-8575; [4]Investigative Treatment Division, Research Center for Innovative Oncology, National Cancer Center Hospital East, Kashiwa, Chiba 277-8577, Japan; [5]CIC-INSERM 00-04, EA 4274, CHU Hôtel Dieu, Nantes, cedex 1; [6]Institut des Maladies de l'Appareil Digestif, CHU Hotel Dieu, Nantes, cedex 1, France

(Received July 18, 2008/Revised August 21, 2008/Accepted August 24, 2008/Online publication November 19, 2008)

Cell permeabilization using microbubbles (MB) and low-intensity ultrasound (US) have the potential for delivering molecules into the cytoplasm. The collapsing MB and cavitation bubbles created by this collapse generate impulsive pressures that cause transient membrane permeability, allowing exogenous molecules to enter the cells. To evaluate this methodology *in vitro* and *in vivo*, we investigated the effects of low-intensity 1-MHz pulsed US and MB combined with *cis*-diamminedichloroplatinum (II) (CDDP) on two cell lines (Colon 26 murine colon carcinoma and EMT6 murine mammary carcinoma) *in vitro* and *in vivo* on severe combined immunodeficient mice inoculated with HT29-luc human colon carcinoma. To investigate *in vitro* the efficiency of molecular delivery by the US and MB method, calcein molecules with a molecular weight in the same range as that of CDDP were used as fluorescent markers. Fluorescence measurement revealed that approximately 10^5–10^7 calcein molecules per cell were internalized. US–MB-mediated delivery of CDDP in Colon 26 and EMT6 cells increased cytotoxicity in a dose-dependent manner and induced apoptosis (nuclear condensation and fragmentation, and increase in caspase-3 activity). *In vivo* experiments with xenografts (HT29-luc) revealed a very significant reduction in tumor volume in mice treated with CDDP + US + MB compared with those in the US + CDDP groups for two different concentrations of CDDP. This finding suggests that the US–MB method combined with chemotherapy has clinical potential in cancer therapy. (*Cancer Sci* 2008; 99: 2525–2531)

Microbubbles (MB) have been developed as ultrasound (US) contrast agents with a diameter of less than 10 μm. The components of their shell membrane vary (albumin, lipid, or polymer), and gases such as air or perfluorocarbons are internalized in them.[1–3] These bubbles oscillate non-linearly in an US field and emit harmonic and subharmonic acoustic signals, thereby enabling differentiation between acoustic scattering and vascular signatures. In addition, because these bubbles behave similar to red blood cells, they have been used to evaluate the blood pool and blood flow at the microvascular level.[4]

Microbubbles collapse in the presence of low-intensity US. There is evidence that impulsive pressures generated by either collapsing MB[5,6] or the cavitation bubbles created by this collapse may permeabilize the plasma membrane of neighboring cells.[7,8] This process results in the diffusion of nearby exogenous molecules into the cytoplasm and a subsequent biological response.[8–11] Because these impulsive pressures can be induced by high-intensity US,[12,13] substantial thermal and mechanical side effects can be reduced using the US–MB method.

The US–MB method is non-toxic and non-immunogenic, and allows local or systemic administration. This method can be used to deliver exogenous molecules into dividing and non-dividing cells and has been investigated as an approach for *in vivo* gene transfer and molecular delivery.[14–16] In any case, the efficiency of molecular delivery depends on the size of the molecules to be delivered.[17,18] The amount of molecules increases with decreasing molecular weight. Thus, it is expected that this methodology will be useful for therapeutic strategies involving drugs with small molecular sizes. Cis-diamminedichloroplatinum (II) (cisplatin; CDDP) is one of the most effective and commonly used chemotherapeutics, possessing a molecular weight of 300. CDDP has been used for the treatment of many solid tumors, including those of the ovaries, testicles, bladder, lung, and head and neck.[19] Increasing CDDP penetration into the tumor cells could further improve its therapeutic efficacy. In the present study, we estimated the number of CDDP molecules internalized by the US–MB method using calcein molecules with molecular weights in the same range as that of CDDP as fluorescent markers. Subsequently, we assessed the therapeutic potential of the combination of CDDP and US with MB *in vitro* and *in vivo* and demonstrated that this combination induces apoptotic effects, and increases the therapeutic efficacy.

Materials and Methods

In vitro and *in vivo* studies were carried out in accordance with the ethical guidelines approved by Tohoku University.

Cell preparation. Human embryonic kidney (293T) cells were a generous gift from Dr Ono of Tohoku University. Murine mammary carcinoma (EMT6) cells were obtained from the American Type Culture Collection (Rockville, MD, USA). Murine colon carcinoma (Colon 26) cells were obtained from the Cell Resource Center for Biomedical Research of the Institute of Development, Aging and Cancer, Tohoku University (Sendai, Japan). Human colon carcinoma (HT-29-luc) cells stably transfected with a plasmid carrying the firefly luciferase gene driven by a cytomegalovirus promoter were obtained from Xenogen (Alameda, CA, USA). Colon 26 and HT-29-luc cells were cultured under standard conditions in RPMI-1640 medium supplemented with 10% heat-inactivated fetal bovine serum (Invitrogen, Carlsbad, CA, USA) and 1% L-glutamine–penicillin–streptomycin (Sigma-Aldrich, St Louis, MO, USA), whereas 293T and EMT6 cells were cultured in Dulbecco's modified Eagle's medium (Sigma-Aldrich) containing the same supplements as those added to the RPMI-1640 medium. HT29-luc cells were selected in 1 mg/mL geneticin (G418) (Sigma-Aldrich). Cells cultured in a 10-cm culture dish were maintained in a humidified incubator at 37°C under an atmosphere containing 5% CO_2 and

[7]To whom correspondence should be addressed.
E-mail: kodama@bme.tohoku.ac.jp

doi: 10.1111/j.1349-7006.2008.00989.x

95% air. The total cell counts and viability were counted in a hemocytometer by the trypan blue dye exclusion method[20] prior to US exposure. Only cells in their exponential growth phase with a viability ≥99% were used for the study.

Microbubbles. MB were created in an aqueous dispersion of 2 mg/mL 1,2-distearoyl-sn-glycero-3-phosphocholine (Avanti Polar Lipids, Alabaster, AL, USA) and 1 mg/mL polyethylene glycol 40 stearate (Sigma-Aldrich) using a 20-kHz sonicator (Vibra Cell; Sonics and Materials, Danbury, CT, USA) in the presence of C_3F_8 gas.[21] The lipid molecules that formed components of the MB surface were confirmed by staining the molecules with 3 μmol/L FM1-43 (excitation 479 nm, emission 598 nm; Molecular Probes, Eugene, OR, USA) and observing them under an inverted microscope (IX81; Olympus, Tokyo, Japan). The peak diameter and the zeta potential of the MB were determined to be 1272 ± 163 nm ($n = 7$) and −4.1 ± 0.85 mV ($n = 3$), respectively, by using a laser diffraction particle size analyzer (particle range 0.6 nm–7 μm; ELSZ-2; Otsuka Electronics, Osaka, Japan).

Ultrasound exposure. Three 1-MHz submersible US probes were used. A 12-mm (Fuji Ceramics, Fujinomiya, Japan) and a 30-mm diameter probe (BFC Applications, Fujisawa, Japan) were used for the *in vitro* experiments, whereas 38-mm diameter probes (Fuji Ceramics) were used for the *in vivo* experiments. Each probe was placed in the test chamber (380 mm × 250 mm × 130 mm) that was previously filled with tap water. Signals of 1 MHz were generated by a multifunction synthesizer (WF1946A; NF Co., Yokohama, Japan) and amplified with a high-speed bipolar amplifier (HSA4101; NF Co.). The pressure values were measured using a polyvinylidene fluoride (PVDF) needle hydrophone (PVDF-Z44-1000; Specialty Engineering Associates, Soquel, CA, USA) at a stand-off distance of 1 mm from the transducer surface by using a stage control system (Mark-204-MS; Sigma Koki, Tokyo, Japan). The signals from both the amplifier and the hydrophone were recorded onto a digital phosphor oscilloscope (Wave Surfer 454, 500 MHz, 1 MΩ [16 pF]; LeCroy Co., Chestnut, NY, USA) in top water degassed with transducer (SPN-620) generated by ultrasonic generator α2 (GP-622D) (Tiyoda Electric Co., Chikuma, Japan). The positive and negative peak values of the pressures were the same. Two intensities, 0.5 and 1.0 W/cm^2, were used in the *in vitro* experiments. The duty cycle was 50%, the number of pulses was 2000, the pulse repletion frequency was 250 Hz, and the exposure time was 10 s. For the *in vivo* experiments, the intensity was 3.0 W/cm^2, the duty cycle was 20%, the number of pulses was 200; the pulse repletion frequency was 1000 Hz, and the exposure time was 60 s. The intensity was defined as the average rate of flow of energy through a unit area placed normal to the direction of propagation.

***In vitro* quantization of calcein uptake.** The 293T cells (5×10^4 cells/well) were seeded in complete medium onto 48-well plates and incubated at 37°C in a 5% CO_2 incubator. On the next day, the medium was replaced with fresh medium containing 200 μmol/L calcein (molecular weight 622) (excitation 494 nm, emission 517 nm; Sigma-Aldrich) with and without MB (10% v/v). After US exposure for 10 s, the cells were washed with phosphate-buffered saline (PBS), trypsinized, and collected in a 15-mL conical tube. Thereafter, the cells were washed three times and transferred to a 1.5-mL conical tube in which they were pelleted. The pellets were lysed in 200 μL reporter lysis buffer (Promega, Madison, WI, USA) and subsequently frozen at −80°C for 15 min. The cells were thawed on ice. Each cell lysate was centrifuged at 12 000*g* for 2 min to pellet the cell debris. Twenty microliters of the supernatant was examined for the uptake of fluorescent molecules using Mx3000P software (Stratagene, La Jolla, CA, USA). The fluorescence of these molecules was excited using a quartz tungsten halogen lamp (350–750 nm), and the emission was collected with a 492–516-nm bandpass filter. The fluorescence data were analyzed with MxPro QPCR Software (Stratagene). The total protein content from an aliquot of each sample of supernatant was calculated by establishing albumin standard curves (BCA protein assay kit; Pierce, Rockford, IL, USA). In addition, two other standard curves were utilized: one to determine the total protein content of the cells, and the other to determine the concentration and intensity of the fluorescence. The experiment was carried out with samples and standards in duplicate, and the absorption of the protein was measured at 562 nm using a plate reader (Sunrise; Tecan Austria, Salzburg, Austria) with the data analysis software LS-Plate manager RD 2001 (Win) (Sunrise). The number of equivalent fluorescent molecules per cell was determined from the calibration curves.

Imaging of confocal fluorescence microscopy. The 293T cells (5×10^4 cells/well) were seeded in complete medium onto alternate 48-well plates to prevent US exposure of neighboring cells.[8] On the next day, the medium was replaced with fresh medium (110 μL) containing calcein (200 μmol/L) with and without MB (10% v/v). After US exposure of 10 s, the plates were incubated for 24 h. Thereafter, the cells were washed three times with PBS and trypsinized. Finally, the cell pellet was resuspended in 60 μL propidium iodide (PI) (excitation 536 nm, emission 617 nm; Molecular Probes) (0.7 μg/mL) and incubated at room temperature for 10–15 min. The calcein and PI fluorescence intensities were determined with a confocal microscope (FV1000; Olympus). A ×60 oil-immersion objective lens with a numerical aperture of 1.25 was used. Calcein and PI fluorescence were excited with the 488-nm line of an argon laser. The laser excitation beam was directed to the specimen through a 488-nm dichroic beam splitter. The emitted fluorescence was collected through a 510–550-nm bandpass emission filter in the green channel and a 580-nm longpass filter in the red channel. Computer-generated images of 1-μm optical sections were obtained at the approximate geometric center of the cell as determined by repeated optical sectioning.

***In vitro* delivery of CDDP.** CDDP (molecular weight 300) was donated by Nihon Kayaku (Tokyo, Japan). Colon 26 and EMT6 cells were seeded in complete medium onto 10-cm culture dishes. Both cells were trypsinized, counted, and transferred into 15-mL round tubes at concentrations of 5×10^5 and 3×10^5 cells/mL, respectively. For control samples, 1 mL complete medium was used as the sample solution; for treated samples, the sample solution was mixed with 800 μL complete medium, 100 μL CDDP solution (0.5–1.0 mmol/L), and 100 μL MB solution (7% v/v). Each tube was positioned above a 30-mm diameter US probe that was immersed in tap water and exposed to US (10 s; 0.5 W/cm^2). After exposure, 4 mL PBS was added to each tube and centrifuged for 5 min at 4°C (350*g*). The cells were washed twice with PBS and subsequently seeded in 1 mL complete medium onto 24-well plates. The plates were incubated for 24 h at 37°C in a 5% CO_2 incubator. The cell viability was determined by a 3-(4,5-dimethylthiazol-2-yl)-2, 5-diphenyltetrazolium bromide (MTT) assay as described previously.[22] Each experiment was carried out with five samples. For each experiment, the mean percentage of treated samples was divided by the mean percentage of control samples to obtain the survival fraction. The mean of five survival fractions was calculated for each condition. The survival fraction of each cell line was measured at the CDDP concentration at which the highest statistical significance was obtained.

***In vitro* analysis of apoptosis.** Colon 26 (5×10^4 cells/well) cells were seeded onto alternate 48 wells to prevent the US exposure of neighboring cells.[8] The medium was replaced with fresh medium (110 μL) containing CDDP (1.5 mg) with and without MB (7% v/v). After US exposure, the plates were incubated for 1 h in a 5% CO_2 incubator, supplemented with 390 μL complete medium; subsequently, the plates were incubated for an additional 24 h at 37°C in the same incubator. The final

doi: 10.1111/j.1349-7006.2008.00989.x

concentration of CDDP was 10 μmol/L. The cell viability was determined by an MTT assay as described previously.[22] Staining with 4′,6-diamidino-2-phenylindole (DAPI; Sigma-Aldrich) was carried out for observing nuclear condensation and fragmentation. Twenty-four hours after the addition of CDDP, the cells were washed with PBS, stained with 100 μL DAPI (100 ng/mL) solution, and observed under an inverted microscope (IX 81). DAPI fluorescence of the cell nuclei was visualized by excitation at 330–385 nm with a 420-nm barrier filter. For determining the induction of apoptotic mediator proteins, caspase-3 activity was measured using a colorimetric assay kit (Medical and Biological Laboratories, Woburn, MA, USA) 24 h after the treatment. In brief, the treated cells were collected from 12 wells of the 48-well plates and suspended in cell lysis buffer. Aliquots of protein were incubated in a reaction buffer containing 10 mmol/L dithiothreitol (DTT) at 37°C for 1 h. A p-nitroaniline-conjugated synthetic peptide was used as the substrate. The caspase activity was calculated by measuring the optic absorbance at 400 nm using a plate reader with the data analysis software LS-Plate manager RD 2001 (Win).

***In vivo* therapeutic effects.** To evaluate the antitumor effects of MB, the antitumor effects of CDDP + US and CDDP + US + MB were compared using xenografts of HT29-luc cells. Two CDDP concentrations (0.5 and 1.25 μg/g bodyweight) were used. HT29-luc cells (1×10^6 cells) in 100 μL saline were injected subcutaneously into the right and left flanks of 16 male severe combined immunodeficient mice aged 6–9 weeks (mouse bodyweight was set to 20 g). The mice were assigned randomly into two groups. On days 3, 7, and 10, all mice were injected intratumorally with the following assigned treatments. (i) Four mice received 20 μL CDDP (0.5 μg/μL bodyweight) with 80 μL saline per site following US exposure (CDDP + US), and four others received 20 μL CDDP (0.5 μg/μL bodyweight) with 30 μL saline and 50 μL MB per site following US exposure (CDDP + US + MB). (ii) Four mice received 50 μL CDDP (1.25 μg/μL bodyweight) with 50 μL saline per site following US exposure (CDDP + US), and four others received 50 μL CDDP (1.25 μg/μL bodyweight) with 50 μL MB per site following US exposure (CDDP + US + MB). The tumors were immersed in tap water with a temperature of 37°C, positioned just above the 38-mm diameter US probe, and exposed to US (3.0 W/cm², 60 s). Bioluminescence induced by CDDP + US + MB was normalized with that of CDDP + US at each concentration (0.5 and 1.25 μg/g bodyweight) on days 4, 7, 9, and 11 to provide the antitumor effects of MB.

Bioluminescence imaging. On days 4, 7, 9, and 11, the mice were anesthetized with isoflurane. Subsequently, they were injected intraperitoneally with luciferin (150 μg/g bodyweight) and placed on the *in vivo* imaging system (IVIS100; Xenogen). The bioluminescence signals were monitored at 10-s time intervals after 10 min luciferin administration. The signal intensity was quantified as the sum of all detected photon counts within the region of interest after subtraction of the measured background luminescence. The light intensity closely correlated with the tumor volume (EMT6-luc) up to 100 mm³, at which point the tumor volume was calculated according to the formula $(\pi/6) \times (\text{width})^2 \times (\text{length})$.[21] In the present experiment, all tumors (HT29-luc) with a volume less than 100 mm³ were subjected to treatment.

Statistical analysis. All measurements are expressed as mean ± SEM. An overall difference between the groups was determined by one-way analysis of variance (one-way ANOVA). When the one-way ANOVA results were significant for three samples, the differences between each group were estimated using the Tukey–Kramer test. Simple comparisons of the mean and SEM of the data were carried out using Student's *t*-test. The differences were considered to be significant at $P < 0.05$.

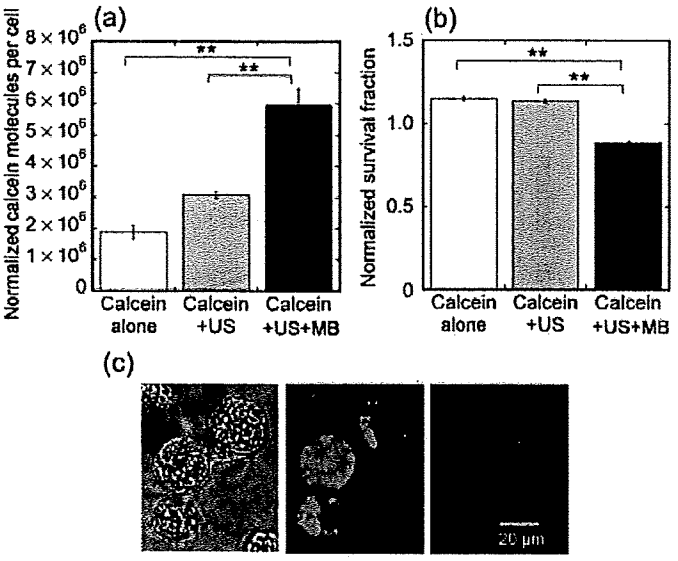

Fig. 1. Uptake of fluorescent molecules by 293T cells. (a) Mean fluorescence uptake under various conditions (calcein alone, calcein + ultrasound [US], and calcein + US + microbubbles [MB]). The calcein + US + MB condition results in a significant increase in the uptake of fluorescent molecules (6.0 ± 0.5 ¥ 106 molecules per cell) compared to calcein alone and calcein + US. Calcein alone (n = 4), calcein + US (n = 4), calcein + US + MB (n = 4). (b) Cell viability measured by the a 3-(4,5-dimethylthiazol-2-yl)-2, 5-diphenyltetrazolium bromide (MTT) assay. The survival fraction is decreased slightly by the effect of US + MB. Calcein alone (n = 4), calcein + US (n = 4), calcein + US + MB (n = 4). (c) Confocal microscopy showing differential interference contrast (left) and fluorescence images (middle) or representative viable 293T cells (right) exposed to US in the presence of MB. Propidium iodide (PI) staining was carried out with fluorescence staining in some cases to confirm that the cells that acquired calcein were viable and excluded PI. Scale bars = 20 mm. Ultrasound intensity 1.0 W/cm2; duty cycle 50%; number of pulses 2000; pulse repletion frequency 250 Hz; and exposure time 10 s. **P < 0.01.

Results

Uptake of fluorescent molecules. Calcein, which has a molecular weight of 622 (calculated stokes radius of 0.68),[23] was used as a fluorescent marker to evaluate small-molecule entry in cancer cells upon US–MB stimulation. As the molecular weight of CDDP is 300 (calculated stokes radius is 0.48 nm), calcein can be considered to represent a realistic marker of CDDP entry into tumor cells.

The exposure of cells to US in the presence of MB resulted in the delivery of 10^6–10^7 calcein molecules per cell (Fig. 1a). This represents a significant increase in the uptake of fluorescent molecules compared to calcein alone and calcein + US. Figure 1b shows that this effect was achieved with a very limited loss of cell viability that was measured by MTT assay, where the survival fraction rate due to MB alone was not investigated as it was found that MB alone did not contribute to cell viability.[24] To confirm that the calcein molecules actually entered the cytoplasm, confocal fluorescence microscopic analysis was carried out. Figure 1c shows the differential interference contrast and fluorescence images or the representative viable 293T cells exposed to US in the presence of MB. PI staining was also carried out with some instances of fluorescence staining to confirm that the cells that acquired calcein were viable and excluded PI. Some cells treated with US in the presence of MB demonstrated intense fluorescence distributed uniformly throughout the entire cell, whereas other cells demonstrated localized intense fluorescence (Fig. 1c).

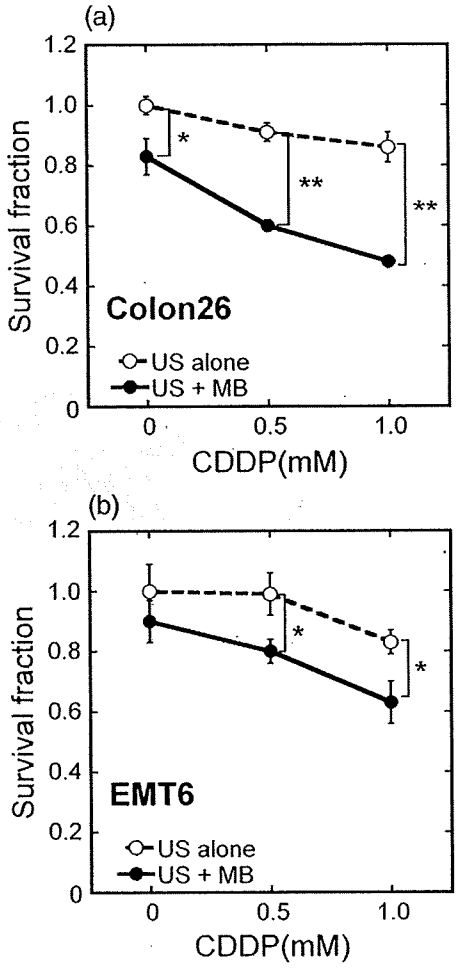

Fig. 2. Potentiation of in vitro cis-diamminedichloroplatinum (II) (CDDP) cytotoxicity in Colon 26 and EMT6 cells. (a) Colon 26: (s) ultrasound (US) alone (n = 5) and (d) US + microbubbles (MB) (n = 5). (b) EMT6: (s) US alone (n = 5) and (d) US + MB (n = 5). Cell survival was measured by a 3-(4,5-dimethylthiazol-2-yl)-2, 5-diphenyltetrazolium bromide (MTT) assay 24 h after US exposure. US intensity 0.5 W/cm2; duty cycle 50%; number of pulses 2000; pulse repletion frequency 250 Hz; and exposure time 10 s. The bars represent mean ± SEM. *P < 0.05, **P < 0.01.

Cytotoxicity *in vitro*. The cytotoxicity of various doses of CDDP in the presence of US with and without MB was tested on Colon 26 and EMT6 cells (Fig. 2). A marked increase in CDDP toxicity was observed under the US–MB conditions, whereas US alone did not significantly affect cell survival with various CDDP concentrations. The CDDP toxicity depended slightly on the cell type.

Apoptosis assay. CDDP is known to induce apoptosis.[25] We confirmed the involvement of apoptosis in mediating cytotoxicity in response to CDDP. Cells undergoing apoptosis demonstrate characteristic nuclear morphological changes with DAPI staining. Figure 3 shows phase contrast and DAPI images of Colon 26 cells. Untreated control cells (Fig. 3a,b) and cells treated with US + MB (Fig. 3c,d), CDDP alone (Fig. 3e,f), and CDDP + US (Fig. 3g,h) showed extremely little condensed or fragmented chromatin. The majority of cells treated with CDDP + US + MB (Fig. 3i,j) displayed apoptotic features, including condensed nuclei and nuclear fragmentation.

Induction of caspase-3 has been suggested as a marker of apoptosis.[26] Figure 4 shows that treatment with US + MB activates caspase-3 as compared to treatment with CDDP alone or with CDDP + US. The caspase activity increases with time. Taken together, the data presented in Figures 3 and 4 demonstrate that the CDDP + US + MB combination decreases cell viability and that this reduction in cell survival is associated with increased induction of apoptosis. In the present study, we did not consider the activation of caspase-3 by US because US alone did not contribute to the survival fraction (Fig. 2) and subsequent apoptosis induction (Fig. 3).

***In vivo* therapeutic effects of MB.** From the above *in vitro* experiments, we found that MB associated with US are able to trigger the uptake of small molecules (Fig. 1), thereby inducing antitumor effects (Fig. 2) and apoptosis (Figs 3,4) in conjunction with CDDP. Thereafter, we investigated the *in vivo* antitumor effects of using MB, in cases in which the xenografts of HT29-luc cells were used. We investigated the antitumor effects of CDDP + US + MB on the xenografts with two different CDDP concentrations (0.5 and 1.25 μg/g bodyweight) on days 4, 7, 9, and 11. The luciferase activity for each concentration of CDDP + US + MB was normalized with each concentration of CDDP + US that was administered previously (Fig. 5a) in order to determine the antitumor effects of MB alone. The activities of the MB were recognized after day 7 (second treatment) in both groups. On day 11, a significant reduction was observed in the CDDP + US + MB group compared to the control and US + MB

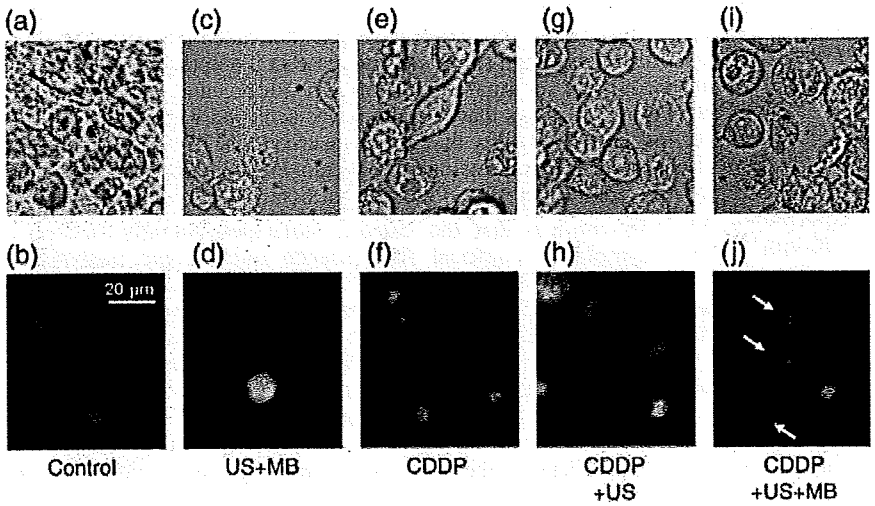

Fig. 3. Nuclear condensation and fragmentation. (a,c,e,g,i) Differential interference contrast and (b,d,f,h,j) 4′,6-diamidino-2-phenylindole (DAPI) fluorescence images of representative viable Colon 26 cells 24 h after treatment. 10 μmol/L cis-diamminedichloroplatinum (II) (CDDP): (a,b) control, (c,d) ultrasound (US) + microbubbles (MB), (e,f) CDDP, (g,h) CDDP + US, and (i,j) CDDP + US + MB. Round or shrunken nuclei of DAPI-stained cells (white arrows) are hallmarks of apoptosis in (j). Experiments were repeated three times with similar results. Scale bar = 20 μm. Ultrasound intensity 1.0 W/cm^2; duty cycle 50%; number of pulses 2000; pulse repletion frequency 250 Hz; and exposure time 10 s.

doi: 10.1111/j.1349-7006.2008.00989.x

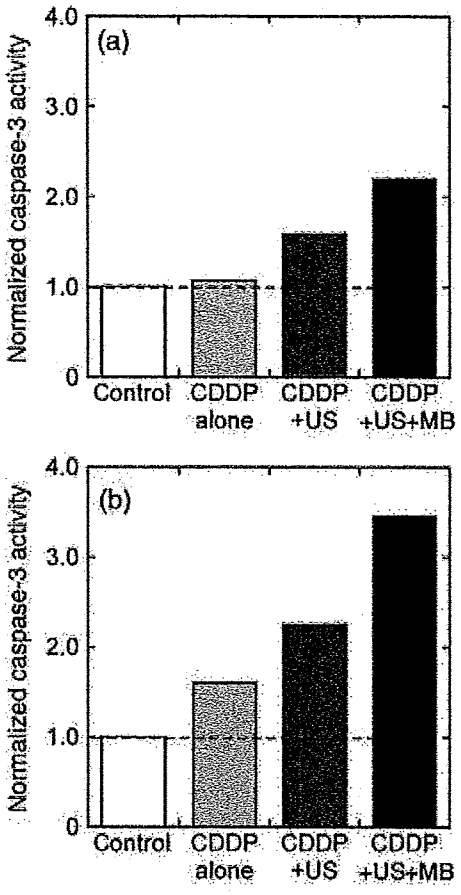

Fig. 4. Upregulation of the proapoptotic gene caspase-3. Colon 26 cells were treated with cis-diamminedichloroplatinum (II) (CDDP) (10 μmol/L) in the presence of ultrasound (US) with and without microbubbles (MB). Caspase-3 activity was measured at 24 h after treatment. Twelve wells from 48-well plates were analyzed for each condition. Results are expressed as the number of molecules of p-nitroaniline (pNA) (nmol) released by 1 mg of protein in (a) 1 and (b) 2 h. Ultrasound intensity 1.0 W/cm²; duty cycle 50%; number of pulses 2000; pulse repletion frequency 250 Hz; and exposure time 10 s.

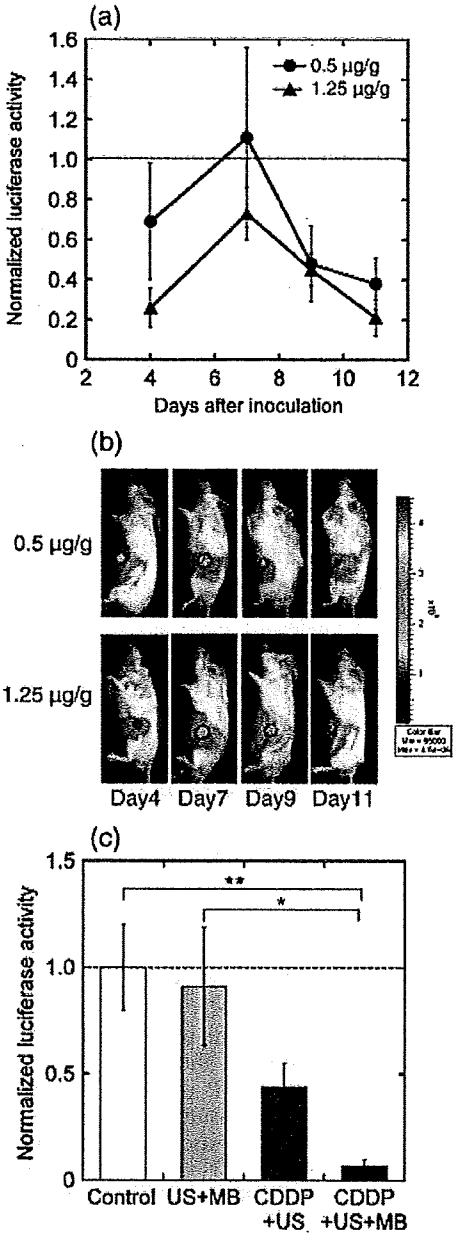

Fig. 5. Antitumor effects of cis-diamminedichloroplatinum (II) (CDDP) + ultrasound (US) + microbubbles (MB) on HT29-luc xenografts with two different CDDP concentrations (0.5 and 1.25 μg/g bodyweight) on days 4, 7, 9, and 11. Ultrasound intensity 3.0 W/cm²; duty cycle 20%; number of pulses 200; pulse repletion frequency 1000 Hz; and exposure time 60 s. Luciferase activity after (a) treatment and (b) bioluminescence imaging. The luciferase activity under each concentration of CDDP + US + MB was normalized with each concentration of CDDP + US. CDDP (0.5 μg/g bodyweight) + US ($n = 4$), CDDP (0.5 μg/g bodyweight) + US + MB ($n = 4$), CDDP (1.25 μg/g bodyweight) + US ($n = 4$), CDDP (1.25 μg/g bodyweight) + US + MB ($n = 4$). (c) The luciferase activity normalized with that of control at day 11, where the concentration of CDDP was 1.25 μg/g bodyweight. Control ($n = 5$), US + MB ($n = 4$). The bars represent mean ± SEM. *$P < 0.05$, **$P < 0.01$.

groups. These effects were recognized by bioluminescence images (Fig. 5b). Figure 5c shows antitumor effects for different conditions (US + MB, CDDP + US, CDDP + US + MB) at day 11, where the CDDP concentration was 1.25 μg/g bodyweight, and the bioluminescence of each condition was normalized with that of the control at day 11. There was no significant difference between control and US + MB. CDDP alone was recognized as the difference between US + MB and CDDP + US, where CDDP alone decreased US + MB by 48.4%. MB further reduced CDDP + US by 84.1%.

Discussion

The US–MB method permeabilizes the cell membrane directly, thereby allowing the delivery of exogenous molecules into the cells. Electroporation is also a method that is used to permeabilize the cell membrane by direct application of an external electric field. Cemazar *et al.* delivered CDDP into both murine sarcoma cisplatin-sensitive TBL.C12 cells and their resistant subclones, namely, TBL.C12.Pt cells.[27] These cells were treated *in vivo* by electroporation, and their platinum content was measured by atomic absorption. Based on their findings, the authors suggested that 10^6 platinum molecules were delivered into TBL.C12 and TBL.C12.Pt cells at 0.05 and 0.46 μg/mL, respectively, where these concentrations correspond to the 50% inhibitory concentration values of platinum for these cells. Our finding that 10^6–10^7 calcein molecules were internalized per cell at 200 μmol/L, as shown in Figure 1a, is in agreement with the finding of Cemazar *et al.* and demonstrates that US–MB permeabilization is as efficient as electroporation in the permeabilization of cell membranes.

There are several anticancer drugs with a similar molecular weight to CDDP. For example, the molecular weight of vincristine is 923, and that of taxol is 854. There is not even one order difference between these molecules and cisplatin, which has a molecular weight of 300. Therefore, we think that the same number of molecules will be delivered into cells by this method. However, it is noted that the number of molecules internalized is not directly correlated with subsequent antitumor effects.

Following the application of MB and US, the cell membrane surface becomes rough and is characterized by depressions that are reversible within 24 h after US exposure.[28,29] Collapsed MB or cavitation bubbles generated by collapsed MB induce impulsive pressures such as liquid jets and shock waves; these pressures affect the neighboring cells. The shock wave propagation distance from the center of a cavitation bubble that has the potential to damage the cell membrane is considerably larger than the maximum radius of the cavitation bubble.[8] Molecular dynamic simulation has revealed that the cell membrane affected by the shock wave is deformed, thereby allowing the entry of exogenous molecules into the cells.[30] Although the membrane permeabilization time has not been measured accurately, it has been reported that the membrane reseals within 80 s when it is permeabilized by shock waves.[31] When 1176 water molecules are delivered into a lipid bilayer comprising 128 dipalmitoylphosphatidylcholine molecules, a water pore of 1.9-nm diameter is formed in the lipid bilayer;[30] this water pore is larger than the CDDP with a diameter of 0.48 nm.

As shown in Figure 1, the US–MB method enhances cell permeability, thereby allowing the delivery of a large number of CDDP molecules into the cells. The combination of high-intensity ultrasound (shock waves) and generated cavitation bubbles – the same concept as that used in the US–MB method – can deliver CDDP molecules into the cells.[32–35] However, the cytotoxicity of CDDP depends on the cell type (Fig. 2); therefore, resistance to CDDP is not completely overcome simply by the application of US and MB (or cavitation bubbles).

The delivery of CDDP into cells induces apoptosis.[36] Apoptotic pathways involved in mediating CDDP-induced cellular effects have been investigated thoroughly.[37] The apoptotic induction resulting from CDDP delivery was confirmed by DAPI staining (Fig. 3) and measurement of caspase-3 activity (Fig. 4). The upregulation of caspase-3 coincides with the observations of previous reports.[10,11,38,39] Caspase-3 is a key effector of apoptosis that is responsible for the proteolytic cleavage of cytoskeletal proteins, kinase, and DNA repair enzymes.[40] The signaling pathway that mediates US-induced apoptosis has been investigated previously.[11,41]

In the *in vivo* experiments, CDDP and MB were injected intratumorally on days 3, 7, and 10 after the injection with tumor cells (HT29-luc), and the tumor was exposed to US. The normalized luciferase activity increased by day 7 and decreased afterwards. This indicates that the antitumor effects resulted from the activity of MB becoming dominant against the tumorigenesity. Tumor growth was suppressed effectively, indicating that the US–MB method provides a synergistic effect with antitumor drugs.[42,43]

We used a local administration system in the *in vivo* experiments (direct injection of CDDP + MB and local US exposure). This local exposure to US has more advantages than the currently available local therapies such as surgery and radiotherapy. However, the usefulness of local therapy is expected to be limited to a particular tumor or a particular tumor stage. For example, hepatocellular carcinomas and brain gliomas seldom metastasize to other organs. Instead, hepatocellular carcinomas and gliomas grow within the liver and brain, respectively, and eventually cause death without metastasizing to other organs. Because these tumors are fed by a tumor-feeding artery, the arterial injection of any anticancer agent (ACA) into the tumor-feeding artery is the most direct way of delivering it into the tumors, mainly because of the first-path effect. With regard to superficial bladder cancer recurrences, half of all such cases recur, and 10–30% progress to a higher grade or stage and form local invasive cancer. Intravesical administration of ACA is known to prolong the duration of progression-free survival. For a clinically randomized phase III trial conducted in patients with stage III ovarian cancer, local intraperitoneal injection of ACA can prolong the duration of overall survival, compared to systemic intravenous injection.[44]

According to the above mentioned evidence, we believe that it is possible to establish a local ACA delivery system in experimental animal models in anticipation of future clinical trials. The US–MB method has the advantages of tissue specificity and non-invasiveness. In addition, this method can be applied repeatedly to patients without immunogenicity.[21] However, the efficiency of molecular delivery into cells is low, and the subsequent bioeffects are not adequate to be investigated by clinical trials. Recently, many types of MB with characteristics of tissue specificity and drug incorporation have been developed[45] and the US exposure conditions have been investigated.[46,47] Combination of the US–MB method with other physical methods such as hyperthermia has also been investigated.[48] In our laboratory, we have investigated the relationship between the physicochemical properties (zeta potential, size, and lipid components) of MB and the transfection efficiency (data not shown).

In conclusion, in the present study we have demonstrated that the US–MB method combined with the well-known chemotherapeutic agent CDDP has great therapeutic potential in cancer therapy. By reducing the dose of CDDP required to induce cell death through the abovementioned method it may be possible to increase the therapeutic action of the drug and to limit the toxicity of the treatment.

Acknowledgments

We thank Fuki Oosawa for her technical assistance. S.M. acknowledges Grant-in-Aid for Scientific Research (B) (19390507) and H.M. acknowledges Grant-in-Aid for Scientific Research (B) (19592334). G.V. acknowledges the program and projects grants from Cancer Research, UK, Institut national de la santé et de la recherche médicale (INSERM), Ligue Contre le Cancer and support through grant 0607-3D1615–66/AO INSERM from the French National Cancer Institute. T.K. acknowledges Grant-in-Aid for Scientific Research (B) (20300173), and Grant-in-Aid for Scientific Research on Priority Area MEXT (20015005). Y.M. and T.K. acknowledge Grant for Research on Nanotechnical Medical, the Ministry of Health, Labour, and Welfare of Japan (H19-nano-010). G.V. and T.K. acknowledge the Japan–France Integrated Action Program Joint Project. CDDP was donated by Nihon Kayaku (Tokyo, Japan).

References

1 Klibanov AL. Ligand-carrying gas-filled microbubbles: ultrasound contrast agents for targeted molecular imaging. *Bioconjug Chem* 2005; **16**: 9–17.
2 Harvey CJ, Blomley MJ, Eckersley RJ, Cosgrove DO. Developments in ultrasound contrast media. *Eur Radiol* 2001; **11**: 675–89.
3 Barak M, Katz Y. Mcirobubbles: pathophysiology and clinical implications. *Chest* 2005; **128**: 2918–32.
4 Lindner JR. Molecular imaging with contrast ultrasound and targeted microbubbles. *J Nucl Cardiol* 2004; **11**: 215–21.
5 Chen WS, Matula TJ, Crum LA. The disappearance of ultrasound contrast bubbles: observations of bubble dissolution and cavitation nucleation. *Ultrasound Med Biol* 2002; **28**: 793–803.

doi: 10.1111/j.1349-7006.2008.00989.x

6 Miller DL, Dou C. Membrane damage thresholds for 1- to 10-MHz pulsed ultrasound exposure of phagocytic cells loaded with contrast agent gas bodies *in vitro*. *Ultrasound Med Biol* 2004; **30**: 973–7.
7 Hallow DM, Mahajan AD, McCutchen TE, Prausnitz MR. Measurement and correlation of acoustic cavitation with cellular bioeffects. *Ultrasound Med Biol* 2006; **32**: 1111–22.
8 Kodama T, Tomita Y, Koshiyama K, Blomley MJ. Transfection effect of microbubbles on cells in superposed ultrasound waves and behavior of cavitation bubble. *Ultrasound Med Biol* 2006; **32**: 905–14.
9 Feril LB Jr, Tsuda Y, Kondo T *et al.* Ultrasound-induced killing of monocytic U937 cells enhanced by 2,2′-azobis (2-amidinopropane) dihydrochloride. *Cancer Sci* 2004; **95**: 181–5.
10 Firestein F, Rozenszajn LA, Shemesh-Darvish L, Elimelech R, Radnay J, Rosenschein U. Induction of apoptosis by ultrasound application in human malignant lymphoid cells: role of mitochondria–caspase pathway activation. *Ann NY Acad Sci* 2003; **1010**: 163–6.
11 Honda H, Kondo T, Zhao QL, Feril LB Jr, Kitagawa H. Role of intracellular calcium ions and reactive oxygen species in apoptosis induced by ultrasound. *Ultrasound Med Biol* 2004; **30**: 683–92.
12 Chaussy C, Thuroff S, Rebillard X, Gelet A. Technology insight: high-intensity focused ultrasound for urologic cancers. *Nat Clin Pract Urol* 2005; **2**: 191–8.
13 Colombel M, Gelet A. Principles and results of high-intensity focused ultrasound for localized prostate cancer. *Prostate Cancer Prostatic Dis* 2004; **7**: 289–94.
14 Hou CC, Wang W, Huang XR *et al.* Ultrasound–microbubble-mediated gene transfer of inducible Smad7 blocks transforming growth factor-β signaling and fibrosis in rat remnant kidney. *Am J Pathol* 2005; **166**: 761–71.
15 Shimamura M, Sato N, Taniyama Y *et al.* Gene transfer into adult rat spinal cord using naked plasmid DNA and ultrasound microbubbles. *J Gene Med* 2005; **7**: 1468–74.
16 Takahashi M, Kido K, Aoi A, Furukawa H, Ono M, Kodama T. Spinal gene transfer using ultrasound and microbubbles. *J Control Release* 2007; **117**: 267–72.
17 Gambihler S, Delius M, Ellwart JW. Permeabilization of the plasma membrane of L1210 mouse leukemia cells using lithotripter shock waves. *J Membr Biol* 1994; **141**: 267–75.
18 Kodama T, Doukas AG, Hamblin MR. Shock wave-mediated molecular delivery into cells. *Biochim Biophys Acta* 2002; **1542**: 186–94.
19 Boulikas T, Vougiouka M. Cisplatin and platinum drugs at the molecular level. *Oncol Reports* 2003; **10**: 1663–82.
20 Tennant JR. Evaluation of the trypan blue technique for determination of cell viability. *Transplantation* 1964; **2**: 685–94.
21 Aoi A, Watanabe Y, Mori S, Takahashi M, Vassaux G, Kodama T. Herpes simplex virus thymidine kinase-mediated suicide gene therapy using nano/microbubbles and ultrasound. *Ultrasound Med Biol* 2008; **34**: 425–34.
22 Kodama T, Doukas AG, Hamblin MR. Delivery of ribosome-inactivating protein toxin into cancer cells with shock waves. *Cancer Lett* 2003; **189**: 69–75.
23 Kodama T, Hamblin MR, Doukas AG. Cytoplasmic molecular delivery with shock waves: importance of impulse. *Biophys J* 2000; **79**: 1821–32.
24 Kodama T, Tan PH, Offiah I *et al.* Delivery of oligodeoxynucleotides into human saphenous veins and the adjunct effect of ultrasound and microbubbles. *Ultrasound Med Biol* 2005; **31**: 1683–91.
25 Kojima H, Endo K, Moriyama H *et al.* Abrogation of mitochondrial cytochrome *c* release and caspase-3 activation in acquired multidrug resistance. *J Biol Chem* 1998; **273**: 16 647–50.
26 Abraham MC, Shaham S. Death without caspases, caspases without death. *Trends Cell Biol* 2004; **14**: 184–93.
27 Cemazar M, Miklavcic D, Mir LM *et al.* Electrochemotherapy of tumours resistant to cisplatin: a study in a murine tumour model. *Eur J Cancer* 2001; **37**: 1166–72.
28 Duvshani-Eshet M, Adam D, Machluf M. The effects of albumin-coated microbubbles in DNA delivery mediated by therapeutic ultrasound. *J Control Release* 2006; **112**: 156–66.
29 Taniyama Y, Tachibana K, Hiraoka K *et al.* Local delivery of plasmid DNA into rat carotid artery using ultrasound. *Circulation* 2002; **105**: 1233–9.
30 Koshiyama K, Kodama T, Yano T, Fujikawa S. Structural change in lipid bilayers and water penetration induced by shock waves: molecular dynamics simulations. *Biophys J* 2006; **91**: 2198–205.
31 Lee S, Anderson T, Zhang H, Flotte TJ, Doukas AG. Alteration of cell membrane by stress waves *in vitro*. *Ultrasound Med Biol* 1996; **22**: 1285–93.
32 Barlogie B, Corry PM, Drewinko B. *In vitro* thermochemotherapy of human colon cancer cells with cis-dichlorodiammineplatinum (II) and mitomycin C. *Cancer Res* 1980; **40**: 1165–8.
33 Weiss N, Delius M, Gambihler S, Eichholtz-Wirth H, Dirschedl P, Brendel W. Effect of shock waves and cisplatin on cisplatin-sensitive and – resistant rodent tumors *in vivo*. *Int J Cancer* 1994; **58**: 693–9.
34 Worle K, Steinbach P, Hofstadter F. The combined effects of high-energy shock waves and cytostatic drugs or cytokines on human bladder cancer cells. *Br J Cancer* 1994; **69**: 58–65.
35 Kambe M, Ioritani N, Shirai S *et al.* Enhancement of chemotherapeutic effects with focused shock waves: extracorporeal shock wave chemotherapy (ESWC). *In Vivo* 1996; **10**: 369–75.
36 Yu T, Huang X, Jiang S, Hu K, Kong B, Wang Z. Ultrastructure alterations in adriamycin-resistant and cisplatin-resistant human ovarian cancer cell lines exposed to nonlethal ultrasound. *Int J Gynecol Cancer* 2005; **15**: 462–7.
37 Siddik ZH. Cisplatin: mode of cytotoxic action and molecular basis of resistance. *Oncogene* 2003; **22**: 7265–79.
38 Honda H, Zhao QL, Kondo T. Effects of dissolved gases and an echo contrast agent on apoptosis induced by ultrasound and its mechanism via the mitochondria–caspase pathway. *Ultrasound Med Biol* 2002; **28**: 673–82.
39 Lagneaux L, de Meulenaer EC, Delforge A *et al.* Ultrasonic low-energy treatment: a novel approach to induce apoptosis in human leukemic cells. *Exp Hematol* 2002; **30**: 1293–301.
40 Li Y, Cohen R. Caspase inhibitors and myocardial apoptosis. *Int Anesthesiol Clin* 2005; **43**: 77–89.
41 Abdollahi A, Domhan S, Jenne JW *et al.* Apoptosis signals in lymphoblasts induced by focused ultrasound. *FASEB J* 2004; **18**: 1413–14.
42 Haag P, Frauscher F, Gradl J *et al.* Microbubble-enhanced ultrasound to deliver an antisense oligodeoxynucleotide targeting the human androgen receptor into prostate tumours. *J Steroid Biochem Mol Biol* 2006; **102**: 103–13.
43 Bekeredjian R, Kuecherer HF, Kroll RD, Katus HA, Hardt SE. Ultrasound-targeted microbubble destruction augments protein delivery into testes. *Urology* 2007; **69**: 386–9.
44 Armstrong DK, Bundy B, Wenzel L *et al.* Intraperitoneal cisplatin and paclitaxel in ovarian cancer. *N Engl J Med* 2006; **354**: 34–43.
45 Suzuki R, Takizawa T, Negishi Y *et al.* Gene delivery by combination of novel liposomal bubbles with perfluoropropane and ultrasound. *J Control Release* 2007; **117**: 130–6.
46 Tartis MS, McCallan J, Lum AF *et al.* Therapeutic effects of paclitaxel-containing ultrasound contrast agents. *Ultrasound Med Biol* 2006; **32**: 1771–80.
47 Rychak JJ, Klibanov AL, Hossack JA. Acoustic radiation force enhances targeted delivery of ultrasound contrast microbubbles: *in vitro* verification. *IEEE Trans Ultrason Ferroelectr Freq Control* 2005; **52**: 421–33.
48 Feril LB Jr, Kondo T. Biological effects of low intensity ultrasound: the mechanism involved, and its implications on therapy and on biosafety of ultrasound. *J Radiat Res (Tokyo)* 2004; **45**: 479–89.

molecular pharmaceutics

Article

Polyplex Micelles with Cyclic RGD Peptide Ligands and Disulfide Cross-Links Directing to the Enhanced Transfection via Controlled Intracellular Trafficking

Makoto Oba, Kazuhiro Aoyagi, Kanjiro Miyata, Yu Matsumoto, Keiji Itaka, Nobuhiro Nishiyama, Yuichi Yamasaki, Hiroyuki Koyama, and Kazunori Kataoka

Mol. Pharmaceutics, **2008**, 5 (6), 1080-1092 • DOI: 10.1021/mp800070s • Publication Date (Web): 08 October 2008

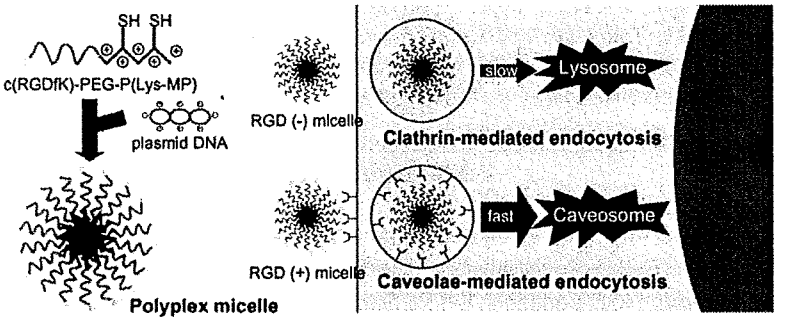

More About This Article

Additional resources and features associated with this article are available within the HTML version:

- Supporting Information
- Access to high resolution figures
- Links to articles and content related to this article
- Copyright permission to reproduce figures and/or text from this article

View the Full Text HTML

Molecular Pharmaceutics is published by the American Chemical Society. 1155 Sixteenth Street N.W., Washington, DC 20036

articles

molecular pharmaceutics

Polyplex Micelles with Cyclic RGD Peptide Ligands and Disulfide Cross-Links Directing to the Enhanced Transfection via Controlled Intracellular Trafficking

Makoto Oba,[†] Kazuhiro Aoyagi,[‡] Kanjiro Miyata,[§,∥] Yu Matsumoto,[⊥] Keiji Itaka,[⊥] Nobuhiro Nishiyama,[∥,⊥] Yuichi Yamasaki,[‡,∥] Hiroyuki Koyama,[†] and Kazunori Kataoka*[,‡,∥,⊥]

Department of Clinical Vascular Regeneration, Graduate School of Medicine, The University of Tokyo, 7-3-1 Hongo, Bunkyo, Tokyo 113-8655, Japan, Department of Materials Engineering, Graduate School of Engineering, The University of Tokyo, 7-3-1 Hongo, Bunkyo, Tokyo 113-8656, Japan, Center for NanoBio Integration, The University of Tokyo, 7-3-1 Hongo, Bunkyo, Tokyo 113-8656, Japan, Department of Bioengineering, Graduate School of Engineering, The University of Tokyo, 7-3-1 Hongo, Bunkyo, Tokyo 113-8656, Japan, and Center for Disease Biology and Integrative Medicine, Graduate School of Medicine, The University of Tokyo, 7-3-1 Hongo, Bunkyo, Tokyo 113-0033, Japan

Received June 24, 2008; Revised Manuscript Received September 16, 2008; Accepted September 23, 2008

Abstract: Thiolated c(RGDfK)-poly(ethylene glycol)-*block*-poly(lysine) (PEG-PLys), a novel block polymer that has a cyclic RGD peptide in the PEG terminus and thiol groups in the PLys side chain, was prepared and applied to the preparation of targetable disulfide cross-linked polyplex micelles through ion complexation with plasmid DNA (pDNA). The obtained polyplex micelles achieved remarkably enhanced transfection efficiency against cultured HeLa cells possessing $\alpha_v\beta_3$ integrin receptors, which are selectively recognized by cyclic RGD peptides, demonstrating the synergistic effect of cyclic RGD peptide ligands on the micelle surface and disulfide cross-links in the core to exert the smooth release of pDNA in the intracellular environment via reductive cleavage. This enhancement was not due to an increase in the uptake amount of polyplex micelles but to a change in their intracellular trafficking route. Detailed confocal laser scanning microscopic observation revealed that polyplex micelles with cyclic RGD peptide ligands were distributed in the perinuclear region in the early stages preferentially through caveolae-mediated endocytosis, which may be a desirable pathway for avoiding the lysosomal degradation of delivered genes. Hence, this approach to introducing ligands and cross-links into the polyplex micelles is promising for the construction of nonviral gene vectors that enhance transfection by controlling intracellular distribution.

Keywords: Polymeric micelle; cyclic RGD peptide; disulfide cross-links; caveolae-mediated endocytosis

Introduction

As an alternative to viral gene vectors with intrinsic safety issues, there is a growing demand for nonviral gene vectors.[1,2] Despite this demand, nonviral gene vectors based on cationic lipids (lipoplexes) and cationic polymers (polyplexes) are still insufficiently for *in vivo* applications, particularly those administered systemically. To achieve

* To whom correspondence should be addressed. Mailing address: The University of Tokyo, Department of Materials Engineering, 7-3-1 Hongo, Bunkyo-ku, Tokyo, 113-8656, Japan. Tel: +81-3-5841-7138. Fax: +81-3-5841-7139. E-mail: kataoka@bmw.t.u-tokyo.ac.jp.

[†] Department of Clinical Vascular Regeneration, Graduate School of Medicine.

[‡] Department of Materials Engineering, Graduate School of Engineering.

[§] Department of Bioengineering, Graduate School of Engineering.

[∥] Center for NanoBio Integration.

[⊥] Center for Disease Biology and Integrative Medicine, Graduate School of Medicine.

10.1021/mp800070s CCC: $40.75
Published on Web 10/08/2008

sufficient *in vivo* systemic transfection, nonviral vectors need to satisfy several properties, such as high stability in the bloodstream, accumulation in target tissues, and controlled intracellular trafficking directing to the nucleus.

Polyplex micelles, composed of poly(ethylene glycol) (PEG)-polycation block copolymers and plasmid DNA (pDNA), are nonviral gene vectors with the potential for systemic application,[3−5] because of the suitable size of approximately 100 nm for systemic administration, and the formation of the biocompatible PEG shell layer to avoid the nonspecific interaction with blood components.[6−8] To further improve the stability and transfection efficiency of polyplex micelles, disulfide cross-links were introduced into the micelle core, revealing the improved transfection to cultured cells as well as the successful reporter gene expression in mouse liver by systemic administration.[9,10] Furthermore, we recently established a procedure to install cyclic RGD peptide ligands (c(RGDfK)), which can selectively recognize $\alpha_v\beta_3$ and $\alpha_v\beta_5$ integrin receptors, on the surface of a polyplex micelle. Eventually, c(RGDfK) installed polyplex micelles exhibited enhanced transfection efficiency against specific cells possessing $\alpha_v\beta_3$ and $\alpha_v\beta_5$ integrin receptors, such as HeLa cells.[11] $\alpha_v\beta_3$ integrin receptors are known to be overexpressed in endothelial cells of tumor capillaries and neointimal tissues. It should be noted that the use of vectors with cyclic RGD peptide ligands has been investigated as an active targeting strategy in antiangiogenic gene therapy for cancer.[12−14] Nevertheless, those studies focused primarily on therapeutic through the facilitation of cellular uptake of the vectors through receptor-mediated routes, and less attention has been paid to the intracellular trafficking of the vectors possibly modulated by the installed ligands. Worth mentioning in this regard is our previous finding that installation of cyclic RGD ligands on the polyplex micelle surface facilitated their localization in the perinuclear region, suggesting the modulated trafficking induced by cyclic RGD ligands.[11]

The study reported here is devoted to get further insights into the modulated cellular uptake and subsequent trafficking of c(RGDfK) installed polyplex micelles in order to enhance transfection efficiency. For this purpose, new polyplex micelles with integrated functions were developed by installing cyclic RGD ligands on the surface and disulfide cross-links in the core. Indeed, the PEG-*block*-poly(lysine) (PEG-PLys) block copolymer as a platform polymer was modified by introducing a cyclic RGD peptide into the PEG terminus as well as thiol groups into the side chain of the PLys segment. The functions of prepared polyplex micelles were tested against HeLa cells possessing $\alpha_v\beta_3$ and $\alpha_v\beta_5$ integrin receptors; the transfection efficiency, the amount of cellular uptake, and the intracellular distribution were thus determined. In particular, the intracellular trafficking of the polyplex micelles loaded with Cy3- or Cy5-labeled pDNA was evaluated thoroughly by confocal laser scanning microscope (CLSM) observation, which clarified the uptake route and the final intracellular localization. The results demonstrated that cyclic RGD ligands facilitated the caveolae-mediated endocytosis of the polyplex micelles and thus improved transfection efficiency, which is apparently important for the design of nonviral gene vectors that can avoid lysosomal degradation. Moreover, cyclic RGD ligands should

(1) Pack, D. W.; Hoffman, A. S.; Pun, S.; Stayton, P. S. Design and Development of Polymers for Gene Delivery. *Nat. Rev. Drug Discovery* **2005**, *4*, 581–593.

(2) Mastrobattista, E.; van der Aa, M. A.; Hennink, W. E.; Crommelin, D. J. A. Artificial Viruses: a Nanotechnological Approach to Gene Delivery. *Nat. Rev. Drug Discovery* **2006**, *5*, 115–121.

(3) Katayose, S.; Kataoka, K. Water-Soluble Polyion Complex Associates of DNA and Poly(ethylene glycol)-Poly(L-lysine) Block Copolymer. *Bioconjugate Chem.* **1997**, *8*, 702–707.

(4) Kakizawa, Y.; Kataoka, K. Block Copolymer Micelles for Delivery of Gene and Related Compounds. *Adv. Drug Delivery Rev.* **2002**, *54*, 203–222.

(5) Osada, K.; Kataoka, K. Drug and Gene Delivery Based on Supramolecular Assembly of PEG-Polypeptide Hybrid Block Copolymers. *Adv. Polym. Sci.* **2006**, *202*, 113–153.

(6) Itaka, K.; Yamauchi, K.; Harada, A.; Nakamura, K.; Kawaguchi, H.; Kataoka, K. Polyion Complex Micelles from Plasmid DNA and Poly(ethylene glycol)-Poly(L-lysine) Block Copolymer as Serum-Tolerable Polyplex System: Physicochemical Properties of Micelles Relevant to Gene Transfection Efficiency. *Biomaterials* **2003**, *24*, 4495–4506.

(7) Han, M.; Bae, Y.; Nishiyama, N.; Miyata, K.; Oba, M.; Kataoka, K. Transfection Study Using Multicellular Tumor Spheroids for Screening Non-Viral Polymeric Gene Vectors with Low Cytotoxicity and High Transfection Efficiencies. *J. Controlled Release* **2007**, *121*, 38–48.

(8) Akagi, D.; Oba, M.; Koyama, H.; Nishiyama, N.; Fukushima, S.; Miyata, T.; Nagawa, H.; Kataoka, K. Biocompatible Micellar Nanovectors Achieve Efficient Gene Transfer to Vascular Lesions without Cytotoxicity and Thrombus Formation. *Gene Ther.* **2007**, *14*, 1029–1038.

(9) Miyata, K.; Kakizawa, Y.; Nishiyama, N.; Harada, A.; Yamasaki, Y.; Koyama, H.; Kataoka, K. Block Catiomer Polyplexes with Regulated Densities of Charge and Disulfide Cross-Linking Directed to Enhanced Gene Expression. *J. Am. Chem. Soc.* **2004**, *126*, 2355–2361.

(10) Miyata, K.; Kakizawa, Y.; Nishiyama, N.; Yamasaki, Y.; Watanabe, T.; Kohara, M.; Kataoka, K. Freeze-Dried Formulations for In Vivo Gene Delivery of PEGylated Polyplex Micelles with Disulfide Crosslinked Cores to the Liver. *J. Controlled Release* **2005**, *109*, 15–23.

(11) Oba, M.; Fukushima, S.; Kanayama, N.; Aoyagi, K.; Nishiyama, N.; Koyama, H.; Kataoka, K. Cyclic RGD Peptide-Conjugated Polyplex Micelles as a Targetable Gene Delivery System Directed to Cells Possessing $\alpha_v\beta_3$ and $\alpha_v\beta_5$ Integrins. *Bioconjugate Chem.* **2007**, *18*, 1415–1423.

(12) Kim, W. J.; Yockman, J. W.; Lee, M.; Jeong, J. H.; Kim, Y. H.; Kim, S. W. Soluble *Flt-1* Gene Delivery Using PEI-*g*-PEG-RGD Conjugate for Anti-Angiogenesis. *J. Controlled Release* **2005**, *106*, 224–234.

(13) Kim, W. J.; Yockman, J. W.; Jeong, J. H.; Christensen, L. V.; Lee, M.; Kim, Y. H.; Kim, S. W. Anti-Angiogenic Inhibition of Tumor Growth by Systemic Delivery of PEI-*g*-PEG-RGD/pCMV-sFlt-1 Complexes in Tumor-Bearing Mice. *J. Controlled Release* **2006**, *114*, 381–388.

(14) Schiffelers, R. M.; Ansari, A.; Xu, J.; Zhou, Q.; Tang, Q.; Storm, G.; Molema, G.; Lu, P. Y.; Scaria, P. V.; Woodle, M. C. Cancer siRNA Therapy by Tumor Selective Delivery with Ligand-Targeted Sterically Stabilized Nanoparticle. *Nucleic Acids Res.* **2004**, *32*, e149.